Published in final edited form as:

Cell Rep. 2025 April 22; 44(4): 115483. doi:10.1016/j.celrep.2025.115483.

PDZD8 promotes autophagy at ER-lysosome membrane contact sites to regulate activity-dependent synaptic growth

Rajan S. Thakur[1,*], **Kate M. O'Connor-Giles**[1,2,3,*]

[1]Department of Neuroscience, Brown University, Providence, RI, USA

[2]Carney Institute for Brain Science, Providence, RI, USA

[3]Lead contact

SUMMARY

Building synaptic connections requires coordinating a host of cellular activities from cell signaling to protein turnover, placing a high demand on intracellular communication. Membrane contact sites (MCSs) formed between organelles have emerged as key signaling hubs for coordinating diverse cellular activities, yet their roles in the developing nervous system remain obscure. We investigate the *in vivo* function of the endoplasmic reticulum (ER) MCS tethering and lipid-transfer protein PDZD8, which was recently linked to intellectual disability, in the nervous system. We find that PDZD8 is required for activity-dependent synaptic bouton formation in multiple paradigms. PDZD8 is sufficient to drive excess synaptic bouton formation through an autophagy-dependent mechanism and required for synapse development when autophagy is limited. PDZD8 accelerates autophagic flux by promoting lysosome maturation at ER-late endosome/lysosome MCSs. We propose that PDZD8 functions in the nervous system to increase autophagy during periods of high demand, including activity-dependent synaptic growth.

In brief

Thakur et al. find that the lipid transfer protein PDZD8 induces synaptic growth. Through *in vivo* studies, the authors find that PDZD8 functions at neuronal ER-late endosome/lysosome membrane contact sites to promote lysosome maturation and accelerate autophagic flux. Increased autophagy in turn induces activity-dependent synapse formation.

Graphical Abstract

*Correspondence: rajan_thakur@brown.edu (R.S.T.), oconnorgiles@brown.edu (K.M.O.-G.).

AUTHOR CONTRIBUTIONS

Conceptualization, R.S.T. and K.M.O.-G.; methodology, R.S.T. and K.M.O.-G.; formal analysis, R.S.T. and K.M.O.-G.; investigation, R.S.T. and K.M.O.-G.; visualization, R.S.T. and K.M.O.-G.; writing – original draft, R.S.T. and K.M.O.-G.; writing – review & editing, R.S.T. and K.M.O.-G.; funding acquisition, K.M.O.-G.; project administration, K.M.O.-G.

DECLARATION OF INTERESTS

The authors declare no competing interests.

SUPPLEMENTAL INFORMATION

Supplemental information can be found online at https://doi.org/10.1016/j.celrep.2025.115483.

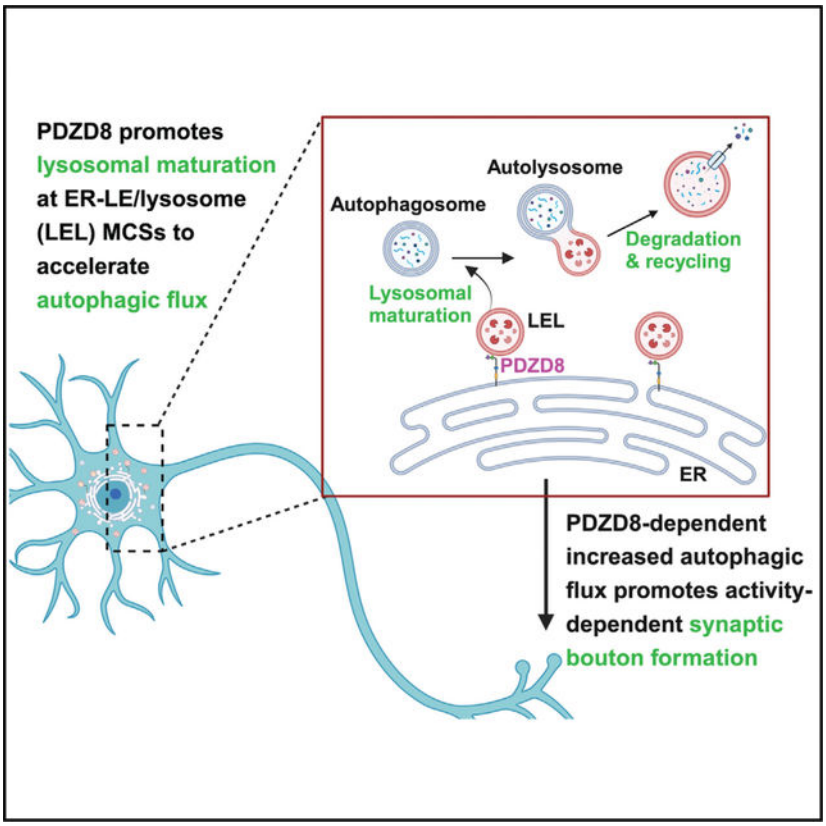

INTRODUCTION

Neurons are large, polarized cells that must coordinate the formation and long-term function of synaptic connections, posing a unique challenge for intracellular communication. Over the last decade, membrane contact sites (MCSs), regions of close apposition between cellular organelles, have been increasingly recognized as key signaling hubs for coordinating a vast array of cellular activities. MCSs are formed by tethering proteins residing in organelle membranes.[1–5] The ER is the largest membrane-bound organelle, forming a network that extends throughout the entire cell, including the distalmost compartments of neurons.[3] The ER interacts with virtually all other cellular organelles through MCSs, enabling communication through the non-vesicular exchange of lipids, ions, and other metabolites for regulating diverse cellular functions.[1–7] While studies over the past decade have led to the identification of MCS tethering factors, including several linked to neurodevelopmental and neurodegenerative disorders, their *in vivo* roles in the nervous system are only beginning to be understood.[8]

In an ongoing effort to identify conserved regulators of synapse formation and function, we identified the resident ER protein PDZD8 as a positive regulator of activity-dependent synaptic bouton formation. PDZD8 is an SMP (synaptotagmin-like mitochondrial-lipid-binding) domain protein belonging to the tubular lipid-binding protein (TULIP) superfamily of lipid transfer proteins. PDZD8 has come to recent attention for its role in tethering multiple ER MCSs.[9–14] PDZD8 was first reported to regulate dendritic Ca^{2+} dynamics in

cultured cortical neurons by promoting ER-mitochondria tethering.[13] More recent studies indicate that a primary PDZD8 function is tethering ER-late endosome/lysosome (LEL) MCSs through interactions with Rab7 and Protrudin.[9–11,14] While the field has gained insight into PDZD8's biochemical role from *in vitro* and cell culture studies, PDZD8's *in vivo* role in neurodevelopment is less clear. PDZD8 appears to play important roles in brain aging *in vivo*[12,15] and in PC12 cells and cultured mouse cortical neurons, PDZD8 knockdown resulted in an overall reduction in neurite outgrowth or reduced axon length, respectively.[10,14] The recent identification of two nonsense variants of *PDZD8* as the cause of autosomal recessive syndromic intellectual disability in multiple families[16] reveals a critical requirement, yet PDZD8's *in vivo* roles in nervous system development remain unknown.

To investigate PDZD8's neurodevelopmental role, we generated genetic reagents in *Drosophila* for *in vivo* studies. We find that PDZD8 is broadly expressed in neurons, where it predominantly localizes to ER-LEL MCSs. PDZD8 is required for the activity-dependent addition of synaptic boutons and sufficient to promote excess synaptic bouton formation. We find that PDZD8 promotes synaptic growth through a macroautophagy-dependent mechanism. Macroautophagy (hereafter referred to as autophagy) is a conserved pathway culminating in the degradation of damaged organelles, protein aggregates, and long-lived proteins in autolysosomes.[17] We find that PDZD8 accelerates autolysosome turnover. Lysosome maturation and, thus, the degradative function of autolysosomes are impaired in the absence of PDZD8. Disruption of PDZD8's C terminus, including its C1 lipid-binding domain, prevents PDZD8 co-localization with LELs, its role in promoting autolysosome turnover, and its ability to induce synaptic bouton formation. Mutation of key residues in the SMP lipid-transfer domain also diminishes PDZD8-induced excess synaptic bouton formation, implicating PDZD8 lipid binding and transfer activity at ER-LEL MCSs. Together our findings support the model that PDZD8 increases autophagic flux to promote synaptic bouton formation during periods of high demand such as activity-dependent synaptic growth.

RESULTS

PDZD8 is required for activity-dependent synaptic bouton formation

We originally identified *PDZD8* as a candidate regulator of synapses based on its transcriptional spatiotemporal expression profile, with high expression during peak synaptogenesis in the developing *Drosophila* embryonic and pupal nervous systems and low expression at other times.[18] We have found that genes with this pattern are enriched for those encoding proteins important for synapse formation and function and are using CRISPR to generate null and endogenously tagged alleles (see STAR Methods) for an ongoing *in vivo* screen of the subset that have not previously been linked to synapse development in any species.[19,20] To investigate PDZD8's potential role in nervous system development, we quantified baseline and activity-dependent synaptic bouton formation at the well-characterized glutamatergic larval neuromuscular junction (NMJ). At NMJs, a single type I motor neuron generally innervates a single muscle cell and forms a stereotyped number of synaptic boutons, each containing ~10 individual active zones

aligned with postsynaptic glutamate receptor clusters.[21] Using anti-HRP, which labels all neuronal membranes, we found that synaptic bouton formation occurs normally in the absence of PDZD8 at the standard rearing temperature of 25°C, indicating that PDZD8 is dispensable for basal synaptic growth under these conditions (Figures 1A and 1B). We next investigated activity-dependent synaptic bouton formation. Previous studies have shown that rearing larvae at elevated temperature leads to activity-induced NMJ expansion due to increased larval locomotion and synaptic activity.[22,23] In wild-type controls, we see an ~40% increase in the number of synaptic boutons in animals reared at 31°C vs. 25°C (Figures 1A and 1B). In contrast, no activity-dependent bouton formation is observed in *PDZD8*^{KO} (Figures 1A and 1B). To confirm that loss of *PDZD8* is responsible for the absence of activity-dependent synaptic bouton formation, we restored a single copy of *PDZD8* under endogenous regulation using a genomic duplication.[24] Restoring PDZD8 function raises bouton number to control levels at 31°C (Figures 1C and 1D), confirming a requirement in activity-dependent synaptic growth *in vivo*. To independently validate PDZD8's role in regulating activity-dependent synaptic bouton formation, we used an acute stimulation paradigm. Previous studies have demonstrated that rapid changes in synaptic activity induced by spaced high-K^+ stimulation rapidly promotes the formation of nascent boutons, which can be identified by the presence of HRP-labeled presynaptic boutons that lack the postsynaptic label Discs large (DLG).[25,26] In wild-type controls labeled for HRP and DLG, we observe significant nascent bouton formation following spaced K^+ stimulation compared with mock stimulation (Figures 1E and 1F). In contrast, spaced K^+ stimulation failed to induce nascent bouton formation in *PDZD8*^{KO} animals (Figures 1E and 1F). Thus, PDZD8 is required for activity-dependent synaptic bouton formation on multiple timescales.

We next sought to determine if PDZD8 is sufficient to induce synaptic growth by driving overexpression of *Drosophila PDZD8* in neurons under the control of the pan-neuronal driver *elav-Gal4*. We observe significant excess bouton formation upon neuronal *PDZD8* overexpression, demonstrating that PDZD8 is sufficient to promote synaptic bouton formation (Figures 1G and 1H). We further find that C-terminal tagging of PDZD8 does not affect overall protein function as pan-neuronal expression of *PDZD8-V5* also promotes excess bouton formation (Figures S1A–S1C). In contrast, expression of PDZD8 in postsynaptic muscle under the control of the driver *24B-Gal4* has no effect on bouton number (Figures 1I and 1J), indicating a presynaptic-specific role for PDZD8 in promoting synaptic bouton formation.

The finding that PDZD8 is sufficient to induce synaptic bouton formation provides an opportunity to assess functional conservation of PDZD8. Human and *Drosophila* PDZD8 share a similar domain structure and 57% amino acid similarity (Figure S1D). We generated a GFP-tagged human *PDZD8* (*hPDZD8-GFP*) transgene and expressed it in neurons. In neuronal cell bodies, hPDZD8-GFP overlaps with PDZD8-V5 in a reticular ER pattern (Figure S1E), consistent with shared regulation. Notably, hPDZD8 induces excess bouton formation similar to *Drosophila* PDZD8 (Figures 1K and 1L). Together, our findings suggest a conserved presynaptic role for PDZD8 in promoting synaptic growth.

PDZD8 promotes synaptic growth via autophagy

The morphology of expanded NMJs induced by *PDZD8* overexpression in neurons, with long branches of small boutons, is strikingly similar to the synaptic overgrowth observed when autophagy is increased,[27] prompting us to investigate potential links between PDZD8 and autophagy. In neurons, autophagy is a constitutive process with diverse roles in synapse formation and maintenance across species.[17,27–37] Neuronal activity also induces autophagy at synapses to maintain protein quality control.[38] Based on the morphological similarity between NMJs overexpressing *PDZD8* or *atg1*, which encodes a kinase critical for coordinating autophagosome formation,[39,40] we hypothesized that the excess bouton formation we observed upon *PDZD8* overexpression may be due to increased autophagy. If so, limiting autophagy should block PDZD8-induced synaptic bouton formation. To test this, we reduced the levels of *atg1* while overexpressing *PDZD8*. We found that loss of a single copy of *atg1* in an otherwise wild-type background does not impact bouton formation (Figures 2A and 2B). However, loss of single copy of *atg1* fully suppressed *PDZD8*-induced bouton formation (Figures 2A and 2B), indicating that PDZD8-induced synaptic bouton formation requires autophagy.

This observation motivated us to test if, in a sensitized background such as *atg1* heterozygotes where levels of a key regulator of autophagy are limiting, PDZD8 is required for synaptic bouton formation. Indeed, reducing *atg1* copy number dominantly enhances loss of *PDZD8*, revealing reduced bouton number when autophagy is limited (Figures 2C and 2D). We observe similar interactions with *syntaxin 17*, which encodes a SNARE protein required for autophagosome-lysosome fusion[41] (Figures S2C–S2F). These findings demonstrate that PDZD8 interacts with the autophagy pathway to positively regulate synaptic bouton formation.

In addition to its role in promoting synaptic bouton formation at the NMJ,[17,27] autophagy also plays key roles in the formation and refinement of individual synapses across species, including in the mouse cortex, fly visual system, and worm NMJs.[28,30,34–37] To investigate the role of PDZD8 and autophagy in the formation of individual synapses, we labeled presynaptic terminals with the active zone marker Brp. Similar to boutons, loss of *PDZD8* alone does not impact the number of active zones per NMJ (Figures 2C and 2E). However, the number of active zones per NMJ is significantly decreased in $PDZD8^{KO}$; $atg1^{PZ}/+$ (Figures 2C and 2E), indicating that PDZD8 promotes synapse formation as well as bouton formation via autophagy. This suggests a requirement for autophagy in active zone formation. However, while autophagy has previously been shown to promote bouton formation,[27] its role in individual motor synapse formation has not been investigated. As predicted, we observe significantly reduced active zone number in homozygous *atg1* mutants, demonstrating that autophagy promotes bouton and synapse formation at the NMJ (Figures 2F–2H). We next investigated whether PDZD8-mediated autophagy is sufficient to induce active zone formation and found that, in contrast to bouton formation, overexpression of *PDZD8* does not affect the total number of active zones per NMJ (Figures S2A and S2B). Together, these findings demonstrate key roles for PDZD8 and autophagy in the formation of boutons and individual motor synapses, and raise the question of how PDZD8 interacts with the autophagy pathway.

PDZD8 promotes autolysosomal turnover

To investigate how PDZD8 promotes autophagy, we quantified autophagic structures labeled by a neuronally expressed mCherry-Atg8a reporter, which marks all autophagic stages,[42] in control and *PDZD8* null mutants. We detect an accumulation of autophagic structures in neuronal cell bodies of *PDZD8* mutants compared with control (Figures 3A–3C). Given mammalian PDZD8's co-localization with LELs, we co-expressed a GFP-Lamp1 reporter[43] to quantify Atg8a+/Lamp1+ autolysosomes.[44] We detect a significant increase in Atg8a+/Lamp1+ structures in $PDZD8^{KO}$ (Figure 3C). The accumulation of autolysosomes in *PDZD8* mutants suggests that PDZD8 may promote autolysosome turnover. To independently confirm these observations and assess autophagy progression, we used a tandem-tagged mCherry-GFP-Atg8a reporter[45] (Figure 3D). Upon transport from autophagosomes to autolysosomes, GFP is rapidly quenched due to the acidic pH, while mCherry persists. Structures positive for both GFP and mCherry (autophagosomes) are not different in $PDZD8^{KO}$ and controls (Figures 3E and 3F, white arrowheads). In contrast, structures positive for mCherry alone (autolysosomes) are significantly increased in $PDZD8^{KO}$, consistent with stalled autolysosome maturation (Figures 3E and 3F, magenta arrowheads). These observations predict that ectopic PDZD8 might accelerate autolysosome turnover. We tested this prediction by overexpressing *PDZD8* in neurons together with mCherry-Atg8a and GFP-Lamp1 reporters. Upon *PDZD8* overexpression, we observe a significant decrease in Atg8a+ and Atg8a+/Lamp1+ structures compared with controls (Figures 3A–3C). Consistently, using the tandem-tagged mCherry-GFP-Atg8a reporter, we find that overexpression of P*DZD8* leads to enhanced clearance of autolysosome structures (Figures 3G and 3H). Consistent with a role for PDZD8 in promoting the clearance of autolysosomal structures, we observed wild-type LEL numbers in neuronal cell bodies upon neuronal overexpression or loss of *PDZD8* (Figures S3A–S3D). Together, these findings support a direct role for PDZD8 in promoting autolysosome turnover.

Autophagy in neurons is compartmentalized with autophagosomes forming in both the cell body and at presynaptic terminals during intense or prolonged neuronal activity.[38,46,47] Autolysosomes formed at terminals are retrogradely transported to the soma for turnover and mature during transport.[29,31–33,36,48] Consistent with a role for PDZD8 acting downstream of autolysosome formation, we observe wild-type autolysosome number at terminals in $PDZD8^{KO}$ and upon neuronal overexpression of *PDZD8* (Figures S3E and S3F). Together, these findings indicate that PDZD8 increases autophagic turnover and suggest that increased autophagic flux is particularly important during activity-dependent synaptic growth.

PDZD8 is enriched in neurons and localizes to ER-LEL MCSs

To better understand the role of PDZD8 in promoting synaptic growth via autophagy, we next investigated PDZD8 cellular and subcellular localization in the nervous system. We generated an endogenously tagged allele of *PDZD8* with V5-mCherry incorporated at the C terminus and confirmed expression of the correct size protein by western blot (Figure S4A). To assess the potential impact of the tag on PDZD8 function, we quantified activity-dependent synapse formation and observed no impairment (Figures S4B and S4C). Thus, endogenous tagging of PDZD8 does not impair its overall function. In the larval nervous system, we observed $PDZD8^{V5\text{-}mCherry}$ expression in cell bodies and the synaptic neuropil

of the ventral ganglion (Figure 4A). To determine which cell types express PDZD8, we co-labeled with antibodies against the neuronal marker Elav and glial marker Repo. We found that PDZD8 appears to be expressed in all neuronal cell bodies, but is not detectable above background in Repo+ glial cells, indicating that PDZD8 is primarily neuronal in the larval nervous system (Figures 4B and 4C). PDZD8 is also expressed at the larval NMJ labeled by the neuronal membrane marker HRP, where it is mostly localized as discrete puncta throughout the presynaptic terminal (Figure 4D).

To better understand PDZD8 subcellular localization, we turned to super-resolution imaging via optical pixel reassignment. We found that both endogenously tagged PDZD8 and neuronally expressed PDZD8-V5 overlap extensively with the ER marker Sturkopf-GFP.[49] PDZD8$^{V5\text{-}mCherry}$ exhibits a punctate pattern expected for ER proteins in fixed cells and similar to that observed in mammalian non-neuronal cells[11,50] (Figure S4D), whereas neuronally expressed PDZD8-V5 exhibits a more reticular pattern (Figure 4E and see Figure S1D). Since PDZD8 encodes a protein reported to localize to multiple ER MCSs, we investigated PDZD8 co-localization with cellular organelles using LEL markers GFP-Rab7 and GFP-Lamp1 and mitochondrial marker GFP-Mito (Figures 4F–4H and S4D–S4G). We observe significant co-localization of PDZD8 and LEL membranes, consistent with recent studies indicating that PDZD8 is enriched at ER-LEL MCSs in non-neuronal cells.[9–11,14] Notably, co-expression of PDZD8-V5 and GFP-Lamp1 leads to an increase in large lysosomal structures, similar to observations in mammalian cells[9,11] (Figure 4G). We also observe PDZD8 co-localizing with ER and ER-LEL MCSs at the larval NMJ (Figures S4H–S4K). We further confirmed ER-lysosome MCS localization of PDZD8 by simultaneously labeling PDZD8, ER, and lysosomes (Figures S5A and S5B). Consistent with prior observations of PDZD8 localization to ER-mitochondrial MCSs,[10,13] we also observe a subset of PDZD8 puncta co-localized with mitochondrial membranes (Figures 4H and S4G). Together, our findings are consistent with the conclusion that PDZD8 is enriched at ER-LEL MCSs in neurons.

PDZD8 localization to ER-LEL MCSs is required to promote autophagy

PDZD8 is a multidomain protein anchored to the ER through an N-terminal transmembrane domain. Following the transmembrane domain, is the SMP lipid-transfer domain, a PDZ protein interaction domain, a C1 lipid-binding domain, and a C-terminal coiled-coil domain that at the sequence level does not appear to be conserved in *Drosophila*[9,14] (Figures S1D and 5A). The C1 domain of mammalian PDZD8 was recently shown to bind a number of phospholipids.[14] To assess the lipid binding ability of the *Drosophila* PDZD8 C1 domain, we incubated strips spotted with phosphatidylinositol phosphate lipids with cell extracts of adult heads expressing V5-tagged full-length PDZD8 (PDZD8-V5) and truncated PDZD8 lacking its C terminus, including the C1 domain, (PDZD8$^{\Delta Cterm}$-V5) in neurons (Figures 5A and S6A). Full-length PDZD8 interacts with phosphatidylserine, phosphatidylinositol (PI), and phosphatidylinositol monophosphates PI3P, PI4P, and PI5P (Figure 5B). With the deletion of the Cterminus, PDZD8's ability to bind lipids is completely lost (Figure 5B), indicating that *Drosophila* PDZD8 also interacts with lipids through its C terminus. We next explored the significance of the Cterminus on the localization of PDZD8 to ER-LEL MCSs *in vivo*. As observed earlier, neuronally expressed PDZD8-V5 localizes

to ER and ER MCSs similar to endogenously tagged PDZD8 (Figure 5C and see Figures 4E–4H). However, deletion of the C terminus specifically abolishes PDZD8 localization to LELs without impacting ER or ER-mitochondrial MCS localization (Figures 5C, 5D, and S6B–S6D). Thus, the C terminus of PDZD8 binds lipids and is required for PDZD8 localization to ER-LEL MCSs in neurons. This observation predicts that the PDZD8 C terminus may be sufficient to localize to LEL membranes. We tested this prediction by expressing full-length PDZD8-V5 and the PDZD8 C terminus (Cterm-V5) in S2R+ cells together with a Lamp1-GFP reporter (Figures S6E and S6F). Consistent with findings in neurons, PDZD8-V5 co-localizes with Lamp1, which we observe in both a punctate and more reticular pattern (Figure S6F). In contrast, Cterm-V5 exhibits diffuse cytoplasmic staining, so, while PDZD8's C terminus is required for recruitment to LEL membranes, we cannot conclude it is sufficient (Figure S6F). Thus, our findings demonstrate a critical role for the C terminus of PDZD8 in LEL targeting in neurons, possibly in conjunction with additional interactions.

This finding allows us to test the functional relevance of ER-LEL MCSs in neurons. To investigate the role of PDZD8 function at ER-LEL MCSs in autophagy, we used the mCherry-Atg8a reporter to quantify overall levels of autophagic structures in neurons overexpressing *PDZD8*$^{\Delta Cterm}$. Whereas overexpression of full-length *PDZD8* once again accelerates the clearance of autophagic intermediates, overexpression of *PDZD8*$^{\Delta Cterm}$ has no effect (Figures 5E and 5F and see Figures 3A–3C). As with full-length *PDZD8* overexpression, overexpression of *PDZD8*$^{\Delta Cterm}$ does not affect LEL number (Figures S6G and S6H). Together, these findings demonstrate that PDZD8's lipid-binding C terminus plays a critical role in linking ER-resident PDZD8 to LELs where it functions to promote autolysosome turnover.

PDZD8 LEL localization and lipid transfer promote synaptic bouton formation

The finding that C terminus-dependent localization of PDZD8 to ER-LEL MCSs is required for PDZD8's role in promoting autolysosome clearance allows us to test the functional relevance of this role in promoting synaptic growth. To do this, we compared the ability of full-length *PDZD8* and *PDZD8*$^{\Delta Cterm}$ to induce bouton formation. Whereas neuronal expression of full-length *PDZD8* induces excess synaptic boutons as expected, overexpression of *PDZD8*$^{\Delta Cterm}$ has no effect on bouton number (Figures 6A and 6B). Thus, we conclude that PDZD8 functions at ER-LEL MCSs to promote synaptic growth via autophagy.

The PDZD8 SMP domain can transport phospholipids *in vitro.*[10,14] To study the functional significance of SMP-dependent lipid transfer activity *in vivo* without disrupting other potential SMP functions,[51] we replaced two conserved SMP domain residues with small hydrophobic side chains (V163 and L271) with tryptophan residues, which have large side chains, to generate a space-filling mutant transgene *PDZD8*^{SMP*} (V163W, L271W; Figures 6C and S1D). These substitutions were previously shown to strongly impair, but not eliminate, lipid transfer in SMP proteins.[10,52] Neuronally expressed *PDZD8*^{SMP*} localizes to ER-LEL and ER-mitochondria MCSs similar to full-length PDZD8 (Figures S7A–S7C and see Figure 4), indicating no requirement for SMP function in localization to MCSs

and allowing us to assess the role of SMP-mediated lipid transfer activity in promoting synaptic bouton formation. Overexpression of *PDZD8*^{SMP*} in neurons significantly reduces PDZD8's ability to induce excess synaptic bouton formation relative to full-length PDZD8 (Figures 6C and 6D). Together, these findings demonstrate *in vivo* roles for PDZD8 lipid binding and transfer activity in promoting synaptic growth.

PDZD8 promotes autolysosome catalytic activity

Given PDZD8's role as an ER-LEL tether, we hypothesized that PDZD8 promotes lysosome maturation and, thus, autolysosome turnover. The tandem-tag reporter assay indicates that autolysosomes acidify, at least to a degree sufficient to quench GFP, in the absence of PDZD8 (see Figures 3D–3H), so we investigated the hydrolytic activity of lysosomes/autolysosomes. The levels of p62 inversely correlate with autophagic degradation in flies and mammals and provide a measure of autolysosome function.[53–55] We find that p62 levels are elevated in *PDZD8*^{KO} (Figures 7A and 7B), consistent with a role for PDZD8 in promoting the degradative activity of autolysosomes. We next labeled adult brains with Magic Red/Green reporters that fluoresce upon cleavage by the lysosomal protease cathepsin B. Magic Red staining is significantly increased upon *PDZD8* overexpression compared with control, whereas overexpression of *PDZD8*$^{\Delta Cterm}$ does not result in increased Magic Red staining (Figures 7C and 7D). Conversely, levels of Magic Green, which we used because our loss-of-function alleles are labeled with a red fluorescent marker, are significantly reduced in *PDZD8*^{KO} compared with wild-type control (Figures 7E and 7F), indicating that the hydrolytic activity of lysosomes is impaired in the absence of PDZD8 function. Thus, PDZD8 functions at ER-LEL MCSs to promote autolysosome catalytic activity.

Taken together, our findings lead to the model that PDZD8 promotes lysosomal maturation to increase autophagic flux and synaptic bouton formation. Specifically, we propose that PDZD8 is required to accelerate autophagy during periods of high demand such as activity-dependent synaptic growth. This suggests that the excess bouton formation induced by Atg1 might require PDZD8-mediated increased autophagic flux. If this is the case, limiting PDZD8 would be predicted to suppress the ability of Atg1 overexpression to induce excess bouton formation. As previously demonstrated,[27] we observe significant NMJ overgrowth when we neuronally express *atg1* under the control of the *elav-Gal4* driver. Loss of a single copy of *PDZD8* has no effect in a wild-type background, but completely suppresses Atg1-induced excess bouton formation (Figure 7H). Together, these findings support the model that PDZD8 promotes lysosome maturation to increase autophagic flux and synaptic growth.

DISCUSSION

The disruption of MCSs underlies a number of neurological disorders, including lysosomal storage disorders, hereditary spastic paraplegia, and neurodegeneration.[56] Mutations in the MCS tethering protein PDZD8 were recently identified as the cause of a rare form of intellectual disability,[16] indicating a critical role in nervous system development. Through

in vivo studies in *Drosophila*, we have found that PDZD8 functions in neurons at ER-LEL MCSs to accelerate autophagy and promote activity-dependent synaptic growth.

We observe accumulation of autolysosomes in neuronal cell bodies in the absence of PDZD8 and reduction upon PDZD8 overexpression, suggesting that PDZD8 accelerates their clearance. The accumulation of autophagy cargo protein p62 in PDZD8 mutants further supports a role in promoting autophagic flux. Our findings indicate that PDZD8 functions at ER-LEL MCSs and downstream of autophagosome-lysosome fusion, pointing to a role in lysosome maturation. Using an mCherry-GFP tandem-tagged Atg8 reporter, which labels mature autolysosomes red due to the quenching of GFP in the low-pH environment, we found that autolysosomes acidify at least partially in *PDZD8* mutants. In contrast, we find that lysosomal protease cathepsin B activity is diminished in *PDZD8* mutants and enhanced upon overexpression of *PDZD8*, indicating a role in promoting the degradative function of lysosomes. Thus, we propose that PDZD8 enhances the degradative capacity of autolysosomes to increase autophagic flux during periods of high demand. The lipid composition of endolysosomes plays an important role in regulating their maturation.[57–59] Given our findings that LEL localization and SMP-dependent lipid transfer are important for PDZD8's roles in neurons, an attractive model is that PDZD8-dependent lipid transport at ER-LEL MCSs regulates the lipid composition of lysosomes to promote the accumulation and/or activation of lysosomal proteases. In COS7 cells, TEX2, another SMP domain-containing lipid transfer protein localized at ER-LEL MCSs, regulates LEL lipid composition and degradative function.[60] A recent study links PDZD8 and TEX2, finding that simultaneous disruption of PDZD8, Tex2, and two $PI(4,5)P_2$ phosphatases results in the accumulation of $PI(4,5)P_2$ on late endosomes and impaired cargo degradation in early *C. elegans* embryos.[61] An intellectual disability-associated *PDZD8* variant is modeled by our $PDZD8^{\Delta Cterm}$ transgenic line, which specifically disrupts localization to ER-LEL MCSs.[16] Thus, loss of PDZD8-dependent lipid transfer at ER-LEL MCSs might lead to ID through the dysregulation of lysosome lipid composition. We and others have found that PDZD8 binds and, *in vitro*, can transfer a number of phosphoinositides and phosphatidylserine.[10,14] In future studies, it will be of great interest to determine how PDZD8 might modulate LEL lipid composition in neurons.

In addition to ER-LEL MCSs, PDZD8 has also been shown to function at neuronal ER-mitochondria MCSs to regulate dendritic Ca^{2+} dynamics and mitochondrial quality control.[12,13] Interestingly, PDZD8 can also form three-way MCSs between ER, LELs, and mitochondria in non-neuronal cells.[9] The extent to which this interaction occurs in the nervous system *in vivo* is unclear. We observe a small fraction of PDZD8 localizing at ER-mitochondrial MCSs in neurons. However, deletion of the C terminus abolishes localization to ER-LEL MCSs without affecting localization to ER-mitochondria MCSs, indicating that PDZD8 recruitment to ER-mitochondria MCSs is independent of its recruitment to ER-LEL MCSs. Our finding that disruption of ER-LEL localization completely suppresses PDZD8's ability to induce synaptic bouton formation suggests that PDZD8 promotes synaptic growth independently of its role at ER-mitochondria MCSs.

The finding that PDZD8 promotes synaptic growth via autophagy adds to a growing understanding of the importance of neuronal autophagy in synapse development, function,

and plasticity.[62–64] Autophagy was first shown to promote bouton formation at the *Drosophila* NMJ through negative regulation of Hiw,[27,65] an E3 ubiquitin ligase that represses the Wnd/DLK pathway.[66] Here, we expand on this work to define a role for autophagy in the formation of individual motor synapses as well. PDZD8's role in basal bouton or synapse formation at the NMJ is only revealed when autophagy is limiting, indicating that it is not required for, but rather enhances or accelerates autophagy. We hypothesize that robust autophagy is particularly important during periods of rapid synaptogenesis. Notably, *Drosophila PDZD8* transcription is highly spatio-temporally regulated with peaks of expression during periods of intense synaptogenesis in embryonic/larval and adult nervous system development.[67] Recent studies in the *Drosophila* visual system underscore the importance of temporally regulated autophagy during circuit formation to ensure stable synapse formation with appropriate partners.[28,30,37] During visual system development, autophagy regulates the abundance of the presynaptic active zone protein Bruchpilot[28] and may target other synaptic building blocks as well. We found that PDZD8 is required for activity-dependent synaptic bouton formation when the requirement for autophagy is likely enhanced, as increased synaptic activity has been shown to induce autophagy across species.[38,68–70] In this context, PDZD8-dependent acceleration of autophagic flux may serve as a mechanism for translating neural activity into new synapse formation. We hypothesize that this may occur through the regulation of synaptic protein abundance and/or activity-dependent growth factor signaling.[27,63,64,71] We also explored the possibility that PDZD8 might act through the regulation of mitophagy but, in agreement with prior findings,[12] observed no effect of PDZD8 overexpression or loss on mitophagy in the larval nervous system (Figures S8A–S8D).

At the *Drosophila* NMJ, VAP33 may also link autophagy and more specifically autolysosome maturation to synaptic growth. Vamp-associated proteins (VAPs) are broad mediators of ER MCSs, including ER-LEL MCSs.[72] Loss of *VAP33/VAPA* results in fewer synaptic boutons and overexpression induces excess formation of small boutons, similar to both *PDZD8* and *atg1.*[73,74] Recent studies in mammals and flies reveal roles for VAPA/B proteins in promoting autophagosome biogenesis at contact sites between ER and isolation membranes (the first step in autophagosome formation) and in lysosome acidification at ER-Golgi MCSs.[75,76] Mutations in multiple genes that disrupt the function or trafficking of v-ATPase, the proton pump responsible for the acidification of lysosomes, alter synapse formation and cause epilepsy and other neurodevelopmental disorders,[77] further linking lysosome/autolysosome maturation and synapse development.

Autophagy also promotes synapse assembly in *C. elegans*, where notably it has distinct roles in different neurons.[35] The regulatory diversity of autophagy in synaptic growth is also revealed by the observation that, in some contexts, autophagy promotes synapse and/or bouton formation,[17,27,34,35] while in others it attenuates synapse formation.[28,30,36,37] These findings point to diverse and context-specific roles for autophagy in sculpting synaptic connections to promote neural circuit formation and function. While autophagy's critical role in neurodegenerative disorders is well established, growing links between regulators of autophagy, including PDZD8, and neurodevelopmental disorders underscore the importance of expanding our understanding of its role in nervous system development and plasticity.

Limitations of the study

In this study, we demonstrate that PDZD8 promotes autophagy-dependent synaptic bouton formation through lipid transfer at ER-LEL MCSs. However, our study does not identify specific lipids transferred or how they promote lysosome maturation and thus autophagic flux. Future analysis of LEL membrane lipid composition in *PDZD8* loss- and gain-of-function backgrounds will help identify lipid species transferred by PDZD8 at neuronal ER-LEL MCSs. We are also unable to determine exactly how PDZD8 is targeted to LELs. While our results demonstrate the critical role of the C terminus, they do not demonstrate that it is sufficient to target PDZD8 to lysosomes, possibly due to an inability to fold properly in isolation or localize properly when overexpressed in S2 cells. Future *in vivo* structure-function studies will be important to map interaction domains and define the roles of lipid and protein interactions in PDZD8 localization to LEL. Finally, our study leaves open the identity of the downstream targets of PDZD8-mediated autophagy that promote synaptic growth.

RESOURCE AVAILABILITY

Lead contact

Requests for any resources or reagents should be addressed to the lead contact, Kate M. O'Connor-Giles (oconnorgiles@brown.edu).

Materials availability

All plasmids, transgenic flies, and custom reagents created for this study are available from the lead contact.

Data and code availability

- The authors declare that the data supporting the findings of this study are available within the paper, Data S1, and supplemental information.
- This study does not report original code.
- Any additional information required to reanalyze the data reported in this paper is available from the lead contact upon request.

STAR★METHODS

EXPERIMENTAL MODEL AND STUDY PARTICIPANT DETAILS

Drosophila stocks: All control genotypes, mutant combinations, and crosses were maintained on cornmeal medium (Fly food R, Lab Express, Ann Arbor, MI) at 25°C and 60% relative humidity with a 12/12 light/dark cycle in specialized incubators (Darwin Chambers, St. Louis, MO). w^{1118} (BDSC#5905) was used as a WT control, unless otherwise noted. The following lines were acquired from the Bloomington Drosophila Stock Center (BDSC, NIH P40OD018537): *UAS-GFP-mCherry-Atg8a* (BDSC#37749), *UAS-mCherry-Atg8a* (BDSC#37750), *UAS-GFP-Lamp1* (BDSC#42714), *UAS-GFP-mito* (BDSC#25748), *UAS-GFP-Rab7* (BDSC#42706), *UAS-Sturkopf-GFP* (BDSC#91394), *PDZD8*-duplication line-$w^{[1118]}$; *Dp(1;3)DC131, PBac(y[+mDint2]*

w[+mC] = DC131)VK00033 (BDSC#30272), *P(PZ) atg1*^{00305}*/TM6* (BDSC#11494), *atg1*^{3}/TM6 (BDSC#60732), *UAS-Atg1* (BDSC#51655), *Syx17*^{f03584}/TM6 (BDSC#85220), *OK6-Gal4* (BDSC#64199), *elav*^{C155}*-Gal4* (BDSC#458), *24B-Gal4* (BDSC#1767) and *UAS-mitoQC* (BDSC#91641).[80] The following genetic lines were generated in this study: *PDZD8*$^{V5\text{-}mCherry}$, *PDZD8*^{KO}, *UAS-PDZD8*, *UAS-PDZD8-V5*, *UAS-hPDZD8-GFP*, *UAS-PDZD8*$^{\Delta Cterm}$ and *UAS-PDZD8*^{SMP*}. All experiments were performed with both male and female animals unless otherwise noted in Table S1. A list of all stocks, their source, and detailed genotypes are listed in the Key Resources Table and Table S1.

METHOD DETAILS

Generation of endogenously tagged and null alleles of *PDZD8*: A CRISPR-based homology directed repair strategy was used to generate in-frame endogenously tagged and null alleles. gRNA target sites were selected using the CRISPR Optimal Target Finder program[81] (http://targetfinder.flycrispr.neuro.brown.edu). gRNA and donor plasmids were generated as described in Bruckner et al., 2017[82] and at flycrispr.com. *Vasa-Cas9* embryos were injected with a mixture of gRNA plasmid (100 ng/μL, each) and a double-stranded DNA donor plasmid (500 ng/μL) by BestGene, Inc., crossed to *w*^{1118} flies following eclosion, and progeny screened for dsRed expression in the eye. All alleles were edited using the scarless CRISPR-piggyBac approach[82] (flycrispr.com). In the first step, a peptide or protein tag flanked by flexible linkers and followed by a visible marker flanked by piggyBac inverted terminal repeat sequences was inserted immediately downstream of the sole *PDZD8* translational start site. This generates a null allele due to interruption of the open reading frame and the presence of stop codons in the visible marker cassette. By crossing edited lines to piggyBac transposase (BDSC#8285), the visible marker cassette can be removed from the germline to generate alleles with in-frame tags. For the endogenous C-terminal V5-mCherry tag, the same approach was used to insert the tag immediately before the sole stop codon. All engineered lines were confirmed by Sanger sequencing of the locus.

Generation of UAS lines: UAS transgenes were generated by cloning full-length or truncated *Drosophila* (Drosophila Genomics Resource Center #1261) or human (provided by Andrés Guillén-Samander and Pietro De Camilli) *PDZD8* cDNAs into pUAST-C5. All transgenes were integrated into the attP2 landing site on the third chromosome (BDSC#8622) by BestGene, Inc. Site-directed mutagenesis was used to introduce the V163W and L271W mutations in UAS-PDZD8$^{SMP*\ (V163W,L271W)}$. All primers used are detailed in the Key Resources Table.

S2R + cell culture and transfections: *Drosophila* S2R + cells were maintained on Schneider's media supplemented with 10% fetal bovine serum and 1.4x Antibiotic-Antimycotic (Thermo Fisher Scientific, USA). Schneider's Line S2 FBtc0000181 (S2-DRSC) cell line used is of D. melanogaster embryonic origin from Drosophila Genomic resource center (DGRC). *Drosophila* S2R + cells are modENCODE authenticated with no mycoplasma contamination and not from the list of commonly misidentified cell lines. Cell transfections were conducted using Effectene (Qiagen #301425) following the manufacturer's protocol and harvested after 48 h for immunohistochemistry.

Immunostaining and confocal imaging: Third-instar larvae were dissected in Ca^{2+}-free saline and fixed for 6 min in Bouin's fixative (Sigma Aldrich, Catalog # HT10132), except for *PDZD8*$^{V5\text{-}mCherry}$, which was fixed in ice-cold methanol for 5 min on ice. Dissected larvae were washed and permeabilized in PBS with 0.1% Triton X-100, blocked in PBS containing 0.1% Triton X-100, 5% NGS and 1% BSA for 30 min at room temperature (RT) or overnight at 4°C, followed by overnight incubation with primary antibodies and 4-h incubation with secondary antibodies at room temperature, then mounted in Vectashield (Vector Laboratories, #H-1000–10). For superresolution imaging, samples were mounted in ProLong Glass Antifade Mountant (ThermoFisher Scientific #P36980) and cured overnight.

S2R + cells were fixed with 2.5% paraformaldehyde for 20 min and permeabilized with 0.37% Igepal for 13 min at room temperature. Cells were blocked using M1 buffer (150mM NaCl, 5mM KCl, 1mM $CaCl_2$, 1mM $MgCl^2$ and 20mM HEPES - pH 6.9) containing 2 mg/ml BSA and 5% NGS for 30 min at room temperature, followed by overnight incubation with primary antibodies at 4°C and 2-h incubation with secondary antibodies at room temperature.

The following primary antibodies were used at the indicated concentrations: Mouse anti-Bruchpilot at 1:100 (Developmental Studies Hybridoma Bank #NC82), Rat anti-Elav at 1:100 (Developmental Studies Hybridoma Bank #7E8A10), Mouse anti-DLG at 1:100 (Developmental Studies Hybridoma Bank #4F3), Mouse anti-GFP at 1:100 (Developmental Studies Hybridoma Bank #12E6), Mouse anti-Repo at 1:25 (Developmental Studies Hybridoma Bank # 8D12), Rabbit anti-RFP at 1:500 (Rockland # 600–401-379), Rat anti-RFP at 1:200 (ChromoTek #5F8), and Mouse anti-V5 at 1:500 (Thermo Fisher Scientific #R960–25). The following Alexa conjugated primary and secondary antibodies were used: Rabbit anti-GFP Alexa Fluor 488 at 1:500 (Thermo Fisher Scientific #A-21311), Anti-HRP conjugated to Cy3 or Alexa Fluor 647 at 1:500 (Jackson ImmunoResearch Laboratories, Inc), and species-specific Alexa Fluor 488/568/647 at 1:500 (Thermo Fisher Scientific). Images were acquired on a Nikon A1R HD confocal microscope with a Plan-Apo 60X 1.49 NA oil-immersion objective at a pixel resolution of 130 nm. Superresolution images were acquired on a Nikon CSU-W1 SoRa (Spinning Disk Super Resolution by Optical Pixel Reassignment) with a Photometrics Prime BSI sCMOS camera and a 60× 1.49 NA oil-immersion objective. Images were acquired using Nikon NIS and deconvolved using Richardson-Lucy deconvolution with 15–20 iterations. Image analysis was performed using the FIJI distribution of ImageJ[83,84] and Nikon Elements General Analysis (GA3) software. Representative images were background subtracted using the rolling ball method and adjusted for brightness and contrast equally across genotypes. Details for all primary and secondary antibodies are in the Key Resources Table.

Lipid-binding analysis: The protocol used was modified from Munnik.et al. for *Drosophila* heads.[85] Approximately 200 heads were prepared in 150μL of fat blot buffer (FBB, 50 mM Tris/Cl-pH 7.5, 150mM NaCl, and freshly added 30ul PIC). Protein extract was centrifuged at 8000 rpm for 15 min at 4°C twice to remove all debris. Total volume was brought to 1 mL with FBB containing 5% BSA. PIP lipid strips (Echelon Biosciences, #P-6001) were blocked with 5% BSA in FBB for 1 h followed by incubation with protein

extracts overnight at 4°C on a nutator. The blots were washed 5 times with 0.1% Tween 20 in FBB for 10 min followed by primary and secondary antibody incubation in FBB containing 0.1% Tween 20 FBB and 5% BSA for 3 h at RT. Blots were washed 5 times with FBB containing 0.1% Tween 20 for 10 min and developed together using an SuperSignal West Femto Maximum Sensitivity Substrate (Thermo Fisher Scientific #34095).

Western blotting: Protein samples were prepared from wandering third instar larval nervous systems or 1-day-old adult fly heads in 2X Laemmli buffer followed by boiling at 95°C for 5 min. Primary antibodies were incubated overnight at 4°C. The following antibodies were used: Rabbit anti-p62 (1:5000, generously provided by Helmut Kramer[79]), Rabbit-anti RFP (1:1000, Rockland 600 401 379), Mouse anti-tubulin (1:4000, Developmental Studies Hybridoma Bank #E7c), and Mouse anti-V5 (1:5000, ThermoFisher Scientific). All HRP-conjugated secondary antibodies (Jackson Immunochemicals) were used at 1:10000 dilutions and incubated for 2 h at room temperature. Blots were developed using SuperSignal West Femto Maximum Sensitivity Substrate (Thermo Fisher Scientific #34095) and imaged on an Azure Biosystems c600. Primary and secondary antibody details are provided in the Key Resource Table.

Activity-induced synaptic bouton formation: The protocol was performed previously as described.[25] Wandering third-instar larvae were dissected in HL3 saline solution (in mM, 70 NaCl, 5 KCl, 0.2 $CaCl_2$, 20 $MgCl_2$, 10 $NaHCO_3$, 5 trehalose, 115 sucrose, and 5 HEPES-NaOH, pH 7.2). The filets were relaxed by moving dissecting pins inward. Filets were then subjected to three 2-min incubations in 90 mm high-K^+ solution (in mM, 40 NaCl, 90 KCl, 1.5 $CaCl_2$, 20 $MgCl_2$, 10 $NaHCO_3$, 5 Trehalose, 5 sucrose, and 5 HEPES-NaOH, pH 7.2), spaced by 10-min incubations in HL3 solution. Following the last high K^+ incubation, larvae were incubated in HL3 solution for 2 min then stretched for fixation and immunostaining. Mock stimulation was performed in parallel in HL3 solution for the same time as K^+ stimulation.

Monitoring Cathepsin B activity with Magic Green/Red: To monitor Cathepsin B activity, dissected adult brains were incubated for 5 min in 1x PBS containing 1x Magic Red cresyl violet-(RR) 2 or for 10 min in 1x PBS containing 1x Magic Green cresyl violet-(RR)2 (Immunochemistry Technology, Bloomington, MN) per manufacturer's instructions and imaged immediately on a Nikon A1R HD confocal microscope with a plan-Apo 40X 1.30 NA oil-immersion objective. Similar brain regions were selected for imaging in all samples.

QUANTIFICATION AND STATISTICAL ANALYSIS

Western blot analysis: Quantification of blots was performed using FIJI/ImageJ software.[83,84,86] The mean background intensities were subtracted from the images. ROIs were drawn around the bands of interest and the integrated intensity of each ROI was extracted from the image. Loading control bands were analyzed in the same manner. Representative images were adjusted linearly across the entire image for brightness and contrast.

Quantification of synaptic bouton and active zone number: Boutons formed by motor neuron 4-Ib on muscle 4 (NMJ 4) of segments A2–4 were labeled with HRP and quantified manually from confocal Z-projections. Nascent boutons were identified as HRP-labeled boutons that lacked DLG staining. NMJ 6/7 was analyzed in abdominal segments 2–4. To analyze the number of active zones per NMJ 4, ROIs were drawn using HRP staining. Nikon Elements Software was used to process images using Gaussian and rolling ball filters and the BrightSpots module, which identifies local maxima based on intensities, was used for segmentation to identify and quantify Brp spots (active zones).

Quantification of Atg8 and Lamp1 puncta: Cell bodies of the larval midline motor neurons were analyzed using Nikon Elements. Images were processed using Gaussian and rolling ball filters, ROIs were manually drawn around individual cell bodies, and the BrightSpots module, which identifies local maxima based on intensities, was used for segmentation to accurately identify and quantify the total number of Atg8a and/or Lamp1 puncta per cell. We used the Atg8a fluorescence signal to create a binary mask to aid in the identification of Atg8a and Lamp1 positive structures.

Quantification of Mander's overlap coefficient: To quantify co-localization, Mander's overlap coefficient was calculated using Just Another Colocalization Plugin (JACoP) in the FIJI distribution of ImageJ[83,84] after manually setting intensity thresholds for both fluorescence channels.

Quantification of Cathepsin B activity with Magic Green/Red: Quantification of Cathepsin B activity was performed using FIJI/ImageJ software.[83,84,86] Multiple ROI's were manually drawn on confocal Z-projection and mean intensities were measured.

Statistical analyses: All experiments were carried out in at least three biological replicates with all crosses set up at least twice to obtain reproducible results from independent replicates. All quantifications were conducted masked to genotype and/or treatment. All graphing and statistical analyses were completed using GraphPad Prism 10. Normally distributed datasets were analyzed using either an unpaired two-sided t test for single comparisons or one-way or two-way ANOVA with Tukey's post hoc test for multiple comparisons. Non-normally distributed datasets were analyzed using either a two-sided Mann–Whitney test for single comparisons or a Kruskal–Wallis test with Dunn's post hoc test for multiple comparisons. Error bars report mean ± SEM. *p* values and statistical tests used are reported in each figure legend and sample sizes with full genotypes are reported in Table S1. All summary statistics are available in Data S1.

Supplementary Material

Refer to Web version on PubMed Central for supplementary material.

ACKNOWLEDGMENTS

We thank FlyBase,[78] BioRender, the Bloomington Drosophila Stock Center (BDSC) (NIH P40OD018537), the Developmental Studies Hybridoma Bank, Dr. Helmut Kramer, Dr. Pietro De Camilli, and Dr. Gábor Juhász for generously providing databases and resources, fly stocks, antibodies, and plasmids used here and in preliminary

experiments. We thank Dr. Arash Bashirullah, Dr. Raghu Padinjat, Dr. Karla Kaun, Dr. Anup Parchure, Dr. Sarah Neuman, and members of the O'Connor-Giles lab for thoughtful discussions and comments on the manuscript. We thank Dr. Mukulika Ray's and Dr. Erica Larschan's laboratory for help with S2R+ cell culture experiments. The Nikon SoRa microscope was generously provided by The Neurobiology of Cells and Circuits/Center for Translational Neuroscience Microscopy Committee, Carney Institute for Brain Science. This work was supported by a grant from the National Institute of Neurological Disorders and Stroke, National Institutes of Health to K.M.O.-G. (R01NS078179) and funds from the Brown University Carney Institute for Brain Science.

REFERENCES

1. Helle SCJ, Kanfer G, Kolar K, Lang A, Michel AH, and Kornmann B (2013). Organization and function of membrane contact sites. Biochim. Biophys. Acta 1833, 2526–2541. 10.1016/j.bbamcr.2013.01.028. [PubMed: 23380708]
2. Phillips MJ, and Voeltz GK (2016). Structure and function of ER membrane contact sites with other organelles. Nat. Rev. Mol. Cell Biol. 17, 69–82. 10.1038/nrm.2015.8. [PubMed: 26627931]
3. Saheki Y, and De Camilli P (2017). Endoplasmic Reticulum–Plasma Membrane Contact Sites. Annu. Rev. Biochem. 86, 659–684. 10.1146/annurev-biochem-061516-044932. [PubMed: 28301744]
4. Salvador-Gallego R, Hoyer MJ, and Voeltz GK (2017). SnapShot: Functions of Endoplasmic Reticulum Membrane Contact Sites. Cell 171, 1224–1224.e1. 10.1016/j.cell.2017.11.005. [PubMed: 29149609]
5. Wu H, Carvalho P, and Voeltz GK (2018). Here, there, and everywhere: The importance of ER membrane contact sites. Science 361, eaan5835. 10.1126/science.aan5835. [PubMed: 30072511]
6. Eden ER (2016). The formation and function of ER-endosome membrane contact sites. Biochim. Biophys. Acta 1861, 874–879. 10.1016/j.bbalip.2016.01.020. [PubMed: 26898183]
7. Raiborg C, Wenzel EM, and Stenmark H (2015). ER–endosome contact sites: molecular compositions and functions. EMBO J. 34, 1848–1858. 10.15252/embj.201591481. [PubMed: 26041457]
8. Kuijpers M, Nguyen PT, and Haucke V (2024). The Endoplasmic Reticulum and Its Contacts: Emerging Roles in Axon Development, Neurotransmission, and Degeneration. Neuroscientist 30, 545–559. 10.1177/10738584231162810. [PubMed: 36960757]
9. Elbaz-Alon Y, Guo Y, Segev N, Harel M, Quinnell DE, Geiger T, Avinoam O, Li D, and Nunnari J (2020). PDZD8 interacts with Protrudin and Rab7 at ER-late endosome membrane contact sites associated with mitochondria. Nat. Commun. 11, 3645. 10.1038/s41467-020-17451-7. [PubMed: 32686675]
10. Gao Y, Xiong J, Chu Q-Z, and Ji W-K (2022). PDZD8-mediated lipid transfer at contacts between the ER and late endosomes/lysosomes is required for neurite outgrowth. J. Cell Sci. 135, 255026. 10.1242/jcs.255026.
11. Guillén-Samander A, Bian X, and De Camilli P (2019). PDZD8 mediates a Rab7-dependent interaction of the ER with late endosomes and lysosomes. Proc. Natl. Acad. Sci. USA 116, 22619–22623. 10.1073/pnas.1913509116. [PubMed: 31636202]
12. Hewitt VL, Miller-Fleming L, Twyning MJ, Andreazza S, Mattedi F, Prudent J, Polleux F, Vagnoni A, and Whitworth AJ (2022). Decreasing pdzd8-mediated mito–ER contacts improves organismal fitness and mitigates Aβ 42 toxicity. Life Sci. Alliance 5, e202201531. 10.26508/lsa.202201531. [PubMed: 35831024]
13. Hirabayashi Y, Kwon S-K, Paek H, Pernice WM, Paul MA, Lee J, Erfani P, Raczkowski A, Petrey DS, Pon LA, and Polleux F (2017). ER-mitochondria tethering by PDZD8 regulates Ca2+ dynamics in mammalian neurons. Science 358, 623–630. 10.1126/science.aan6009. [PubMed: 29097544]
14. Shirane M, Wada M, Morita K, Hayashi N, Kunimatsu R, Matsumoto Y, Matsuzaki F, Nakatsumi H, Ohta K, Tamura Y, and Nakayama KI (2020). Protrudin and PDZD8 contribute to neuronal integrity by promoting lipid extraction required for endosome maturation. Nat. Commun. 11, 4576. 10.1038/s41467-020-18413-9. [PubMed: 32917905]
15. Morita K, Wada M, Nakatani K, Matsumoto Y, Hayashi N, Yamahata I, Mitsunari K, Mukae N, Takahashi M, Izumi Y, et al. (2022). PDZD8-deficient mice accumulate cholesteryl esters

in the brain as a result of impaired lipophagy. iScience 25, 105612. 10.1016/j.isci.2022.105612. [PubMed: 36465123]

16. Al-Amri AH, Armstrong P, Amici M, Ligneul C, Rouse J, El-Asrag ME, Pantiru A, Vancollie VE, Ng HWY, Ogbeta JA, et al. (2022). PDZD8 Disruption Causes Cognitive Impairment in Humans, Mice, and Fruit Flies. Biol. Psychiatry 92, 323–334. 10.1016/j.biopsych.2021.12.017. [PubMed: 35227461]
17. Batlevi Y, Martin DN, Pandey UB, Simon CR, Powers CM, Taylor JP, and Baehrecke EH (2010). Dynein light chain 1 is required for autophagy, protein clearance, and cell death in Drosophila. Proc. Natl. Acad. Sci. USA 107, 742–747. 10.1073/pnas.0907967107. [PubMed: 20080745]
18. Brown JB, Boley N, Eisman R, May GE, Stoiber MH, Duff MO, Booth BW, Wen J, Park S, Suzuki AM, et al. (2014). Diversity and dynamics of the Drosophila transcriptome. Nature 512, 393–399. 10.1038/nature12962. [PubMed: 24670639]
19. Hogan CA, Gratz SJ, Dumouchel JL, Thakur RS, Delgado A, Lentini JM, Madhwani KR, Fu D, and O'Connor-Giles KM (2023). Expanded tRNA methyltransferase family member TRMT9B regulates synaptic growth and function. EMBO Rep. 24, e56808. 10.15252/embr.202356808. [PubMed: 37642556]
20. Kentro JA, Singh G, Pham TM, Currie J, Khullar S, Medeiros AT, Larschan E, and O'Connor-Giles KM (2024). Conserved Transcription Factors Coordinate Synaptic Gene Expression through Repression (Cold Spring Harbor Laboratory).
21. Harris KP, and Littleton JT (2015). Transmission, Development, and Plasticity of Synapses. Genetics 201, 345–375. 10.1534/genetics.115.176529. [PubMed: 26447126]
22. Sigrist SJ, Reiff DF, Thiel PR, Steinert JR, and Schuster CM (2003). Experience-Dependent Strengthening of Drosophila Neuromuscular Junctions. J. Neurosci. 23, 6546–6556. 10.1523/jneurosci.23-16-06546.2003. [PubMed: 12878696]
23. Zhong Y, and Wu CF (2004). Neuronal Activity and Adenylyl Cyclase in Environment-Dependent Plasticity of Axonal Outgrowth in Drosophila. J. Neurosci. 24, 1439–1445. 10.1523/jneurosci.0740-02.2004. [PubMed: 14960616]
24. Venken KJT, Popodi E, Holtzman SL, Schulze KL, Park S, Carlson JW, Hoskins RA, Bellen HJ, and Kaufman TC (2010). A Molecularly Defined Duplication Set for the X Chromosome of Drosophila melanogaster. Genetics 186, 1111–1125. 10.1534/genetics.110.121285. [PubMed: 20876565]
25. Piccioli ZD, and Littleton JT (2014). Retrograde BMP signaling modulates rapid activity-dependent synaptic growth via presynaptic LIM kinase regulation of cofilin. J. Neurosci. 34, 4371–4381. 10.1523/JNEUROSCI.4943-13.2014. [PubMed: 24647957]
26. Ataman B, Ashley J, Gorczyca M, Ramachandran P, Fouquet W, Sigrist SJ, and Budnik V (2008). Rapid Activity-Dependent Modifications in Synaptic Structure and Function Require Bidirectional Wnt Signaling. Neuron 57, 705–718. 10.1016/j.neuron.2008.01.026. [PubMed: 18341991]
27. Shen W, and Ganetzky B (2009). Autophagy promotes synapse development in Drosophila. J. Cell Biol. 187, 71–79. 10.1083/jcb.200907109. [PubMed: 19786572]
28. Dutta SB, Linneweber GA, Andriatsilavo M, Hiesinger PR, and Hassan BA (2023). EGFR-dependent suppression of synaptic autophagy is required for neuronal circuit development. Curr. Biol. 33, 517–532.e5. 10.1016/j.cub.2022.12.039. [PubMed: 36640763]
29. Hollenbeck PJ (1993). Products of endocytosis and autophagy are retrieved from axons by regulated retrograde organelle transport. J. Cell Biol. 121, 305–315. 10.1083/jcb.121.2.305. [PubMed: 7682217]
30. Kiral FR, Linneweber GA, Mathejczyk T, Georgiev SV, Wernet MF, Hassan BA, Von Kleist M, and Hiesinger PR (2020). Autophagy-dependent filopodial kinetics restrict synaptic partner choice during Drosophila brain wiring. Nat. Commun. 11, 1325. 10.1038/s41467-020-14781-4. [PubMed: 32165611]
31. Lee S, Sato Y, and Nixon RA (2011). Lysosomal Proteolysis Inhibition Selectively Disrupts Axonal Transport of Degradative Organelles and Causes an Alzheimer's-Like Axonal Dystrophy. J. Neurosci. 31, 7817–7830. 10.1523/jneurosci.6412-10.2011. [PubMed: 21613495]
32. Maday S, and Holzbaur ELF (2016). Compartment-Specific Regulation of Autophagy in Primary Neurons. J. Neurosci. 36, 5933–5945. 10.1523/jneurosci.4401-15.2016. [PubMed: 27251616]

33. Maday S, Wallace KE, and Holzbaur ELF (2012). Autophagosomes initiate distally and mature during transport toward the cell soma in primary neurons. J. Cell Biol. 196, 407–417. 10.1083/jcb.201106120. [PubMed: 22331844]
34. Rowland AM, Richmond JE, Olsen JG, Hall DH, and Bamber BA (2006). Presynaptic Terminals Independently Regulate Synaptic Clustering and Autophagy of GABA A Receptors in Caenorhabditis elegans. J. Neurosci. 26, 1711–1720. 10.1523/jneurosci.2279-05.2006. [PubMed: 16467519]
35. Stavoe AKH, Hill SE, Hall DH, and Colón-Ramos DA (2016). KIF1A/UNC-104 Transports ATG-9 to Regulate Neurodevelopment and Autophagy at Synapses. Dev. Cell 38, 171–185. 10.1016/j.devcel.2016.06.012. [PubMed: 27396362]
36. Tang G, Gudsnuk K, Kuo S-H, Castagna C, Yamamoto A, Cotrina ML, Rosoklija G, Sosunov A, Sonders MS, Kanter E, et al. (2014). Loss of mTOR-Dependent Macroautophagy Causes Autistic-like Synaptic Pruning Deficits. Neuron 83, 1131–1143. 10.1016/j.neuron.2014.07.040. [PubMed: 25155956]
37. Hernandez-Diaz S, Ghimire S, Sanchez-Mirasierra I, Montecinos-Oliva C, Swerts J, Kuenen S, Verstreken P, and Soukup SF (2022). Endophilin-B regulates autophagy during synapse development and neurodegeneration. Neurobiol. Dis. 163, 105595. 10.1016/j.nbd.2021.105595. [PubMed: 34933093]
38. Soukup S-F, Kuenen S, Vanhauwaert R, Manetsberger J, Hernández-Díaz S, Swerts J, Schoovaerts N, Vilain S, Gounko NV, Vints K, et al. (2016). A LRRK2-Dependent EndophilinA Phosphoswitch Is Critical for Macroautophagy at Presynaptic Terminals. Neuron 92, 829–844. 10.1016/j.neuron.2016.09.037. [PubMed: 27720484]
39. Scott RC, Schuldiner O, and Neufeld TP (2004). Role and Regulation of Starvation-Induced Autophagy in the Drosophila Fat Body. Dev. Cell 7, 167–178. 10.1016/j.devcel.2004.07.009. [PubMed: 15296714]
40. Suzuki K, Kirisako T, Kamada Y, Mizushima N, Noda T, and Ohsumi Y (2001). The pre-autophagosomal structure organized by concerted functions of APG genes is essential for autophagosome formation. EMBO J. 20, 5971–5981. 10.1093/emboj/20.21.5971. [PubMed: 11689437]
41. Takáts S, Nagy P, Varga Á, Pircs K, Kárpáti M, Varga K, Kovács AL, Hegedu}s K, and Juhász G. (2013). Autophagosomal Syntaxin17-dependent lysosomal degradation maintains neuronal function in Drosophila. JCB (J. Cell Biol.) 201, 531–539. 10.1083/jcb.201211160. [PubMed: 23671310]
42. Chang Y-Y, and Neufeld TP (2009). An Atg1/Atg13 Complex with Multiple Roles in TOR-mediated Autophagy Regulation. Mol. Biol. Cell 20, 2004–2014. 10.1091/mbc.e08-12-1250. [PubMed: 19225150]
43. Pulipparacharuvil S, Akbar MA, Ray S, Sevrioukov EA, Haberman AS, Rohrer J, and Krämer H (2005). Drosophila Vps16A is required for trafficking to lysosomes and biogenesis of pigment granules. J. Cell Sci. 118, 3663–3673. 10.1242/jcs.02502. [PubMed: 16046475]
44. Mauvezin C, Ayala C, Braden CR, Kim J, and Neufeld TP (2014). Assays to monitor autophagy in Drosophila. Methods 68, 134–139. 10.1016/j.ymeth.2014.03.014. [PubMed: 24667416]
45. Nezis IP, Shravage BV, Sagona AP, Lamark T, Bjørkøy G, Johansen T, Rusten TE, Brech A, Baehrecke EH, and Stenmark H (2010). Autophagic degradation of dBruce controls DNA fragmentation in nurse cells during late Drosophila melanogaster oogenesis. J. Cell Biol. 190, 523–531. 10.1083/jcb.201002035. [PubMed: 20713604]
46. Shehata M, Matsumura H, Okubo-Suzuki R, Ohkawa N, and Inokuchi K (2012). Neuronal Stimulation Induces Autophagy in Hippocampal Neurons That Is Involved in AMPA Receptor Degradation after Chemical Long-Term Depression. J. Neurosci. 32, 10413–10422. 10.1523/jneurosci.4533-11.2012. [PubMed: 22836274]
47. Stavoe AKH, and Holzbaur ELF (2019). Autophagy in Neurons. Annu. Rev. Cell Dev. Biol. 35, 477–500. 10.1146/annurev-cellbio-100818-125242. [PubMed: 31340124]
48. Cheng X-T, Xie Y-X, Zhou B, Huang N, Farfel-Becker T, and Sheng Z-H (2018). Characterization of LAMP1-labeled nondegradative lysosomal and endocytic compartments in neurons. J. Cell Biol. 217, 3127–3139. 10.1083/jcb.201711083. [PubMed: 29695488]

49. Thiel K, Heier C, Haberl V, Thul PJ, Oberer M, Lass A, Jäckle H, and Beller M (2013). The evolutionary conserved protein CG9186 is associated with lipid droplets, required for their positioning and for fat storage. J. Cell Sci. 126, 2198–2212. 10.1242/jcs.120493. [PubMed: 23525007]
50. Summerville JB, Faust JF, Fan E, Pendin D, Daga A, Formella J, Stern M, and McNew JA (2016). The effects of ER morphology on synaptic structure and function in Drosophila melanogaster. J. Cell Sci. 129, 1635–1648. 10.1242/jcs.184929. [PubMed: 26906425]
51. Nakamura K, Aoyama-Ishiwatari S, Nagao T, Paaran M, Obara CJ, Sakurai-Saito Y, Johnston J, Du Y, Suga S, Tsuboi M, et al. (2023). Mitochondrial Protein FKBP8 Captures PDZD8 to Form Mitochondria-ER Contacts (Cold Spring Harbor Laboratory).
52. Saheki Y, Bian X, Schauder CM, Sawaki Y, Surma MA, Klose C, Pincet F, Reinisch KM, and De Camilli P (2016). Control of plasma membrane lipid homeostasis by the extended synaptotagmins. Nat. Cell Biol. 18, 504–515. 10.1038/ncb3339. [PubMed: 27065097]
53. Devorkin L, and Gorski SM (2014). Monitoring Autophagic Flux Using Ref(2)P, the Drosophila p62 Ortholog. Cold Spring Harbor Protocols *2014*, pdb.prot080333. Cold Spring Harb. Protoc. 2014, 959–966. 10.1101/pdb.prot080333. [PubMed: 25183816]
54. Pircs K, Nagy P, Varga A, Venkei Z, Erdi B, Hegedus K, and Juhasz G (2012). Advantages and Limitations of Different p62-Based Assays for Estimating Autophagic Activity in Drosophila. PLoS One 7, e44214. 10.1371/journal.pone.0044214. [PubMed: 22952930]
55. Jiang P, and Mizushima N (2015). LC3- and p62-based biochemical methods for the analysis of autophagy progression in mammalian cells. Methods 75, 13–18. 10.1016/j.ymeth.2014.11.021. [PubMed: 25484342]
56. Kim S, Coukos R, Gao F, and Krainc D (2022). Dysregulation of organelle membrane contact sites in neurological diseases. Neuron 110, 2386–2408. 10.1016/j.neuron.2022.04.020. [PubMed: 35561676]
57. Ebner M, Puchkov D, López-Ortega O, Muthukottiappan P, Su Y, Schmied C, Zillmann S, Nikonenko I, Koddebusch J, Dornan GL, et al. (2023). Nutrient-regulated control of lysosome function by signaling lipid conversion. Cell 186, 5328–5346.e26. 10.1016/j.cell.2023.09.027. [PubMed: 37883971]
58. Baba T, and Balla T (2020). Emerging roles of phosphatidylinositol 4-phosphate and phosphatidylinositol 4,5-bisphosphate as regulators of multiple steps in autophagy. J. Biochem. 168, 329–336. 10.1093/jb/mvaa089. [PubMed: 32745205]
59. Tang H, Huang X, and Pang S (2022). Regulation of the lysosome by sphingolipids: Potential role in aging. J. Biol. Chem. 298, 102118. 10.1016/j.jbc.2022.102118. [PubMed: 35691340]
60. Du Y, Chang W, Gao L, Deng L, and Ji W-K (2023). Tex2 is required for lysosomal functions at TMEM55-dependent ER membrane contact sites. J. Cell Biol. 222, e202205133. 10.1083/jcb.202205133. [PubMed: 36705603]
61. Jeyasimman D, Ercan B, Dharmawan D, Naito T, Sun J, and Saheki Y (2021). PDZD-8 and TEX-2 regulate endosomal PI(4,5)P2 homeostasis via lipid transport to promote embryogenesis in C. elegans. Nat. Commun. 12, 6065. 10.1038/s41467-021-26177-z. [PubMed: 34663803]
62. Crawley O, and Grill B (2021). Autophagy in axonal and presynaptic development. Curr. Opin. Neurobiol. 69, 139–148. 10.1016/j.conb.2021.03.011. [PubMed: 33940492]
63. Decet M, and Verstreken P (2021). Presynaptic Autophagy and the Connection With Neurotransmission. Front. Cell Dev. Biol. 9, 790721. 10.3389/fcell.2021.790721. [PubMed: 34988081]
64. Hill SE, and Colón-Ramos DA (2020). The Journey of the Synaptic Autophagosome: A Cell Biological Perspective. Neuron 105, 961–973. 10.1016/j.neuron.2020.01.018. [PubMed: 32191859]
65. Tian X, Li J, Valakh V, DiAntonio A, and Wu C (2011). Drosophila Rae1 controls the abundance of the ubiquitin ligase Highwire in post-mitotic neurons. Nat. Neurosci. 14, 1267–1275. 10.1038/nn.2922. [PubMed: 21874015]
66. Collins CA, Wairkar YP, Johnson SL, and Diantonio A (2006). Highwire Restrains Synaptic Growth by Attenuating a MAP Kinase Signal. Neuron 51, 57–69. 10.1016/j.neuron.2006.05.026. [PubMed: 16815332]

67. Graveley BR, Brooks AN, Carlson JW, Duff MO, Landolin JM, Yang L, Artieri CG, Van Baren MJ, Boley N, Booth BW, et al. (2011). The developmental transcriptome of Drosophila melanogaster. Nature 471, 473–479. 10.1038/nature09715. [PubMed: 21179090]
68. Wang T, Martin S, Papadopulos A, Harper CB, Mavlyutov TA, Niranjan D, Glass NR, Cooper-White JJ, Sibarita JB, Choquet D, et al. (2015). Control of autophagosome axonal retrograde flux by presynaptic activity unveiled using botulinum neurotoxin type a. J. Neurosci. 35, 6179–6194. 10.1523/JNEUROSCI.3757-14.2015. [PubMed: 25878289]
69. Bademosi AT, Decet M, Kuenen S, Calatayud C, Swerts J, Gallego SF, Schoovaerts N, Karamanou S, Louros N, Martin E, et al. (2023). EndophilinA-dependent coupling between activity-induced calcium influx and synaptic autophagy is disrupted by a Parkinson-risk mutation. Neuron 111, 1402–1422.e13. 10.1016/j.neuron.2023.02.001. [PubMed: 36827984]
70. Katsumata K, Nishiyama J, Inoue T, Mizushima N, Takeda J, and Yuzaki M (2010). Dynein- and activity-dependent retrograde transport of autophagosomes in neuronal axons. Autophagy 6, 378–385. 10.4161/auto.6.3.11262. [PubMed: 20150763]
71. Deshpande M, and Rodal AA (2016). The Crossroads of Synaptic Growth Signaling, Membrane Traffic and Neurological Disease: Insights from Drosophila. Traffic 17, 87–101. 10.1111/tra.12345. [PubMed: 26538429]
72. Subra M, Dezi M, Bigay J, Lacas-Gervais S, Di Cicco A, Araújo ARD, Abélanet S, Fleuriot L, Debayle D, Gautier R, et al. (2023). VAP-A intrinsically disordered regions enable versatile tethering at membrane contact sites. Dev. Cell 58, 121–138.e9. 10.1016/j.devcel.2022.12.010. [PubMed: 36693319]
73. Pennetta G, Hiesinger PR, Fabian-Fine R, Meinertzhagen IA, and Bellen HJ (2002). Drosophila VAP-33A Directs Bouton Formation at Neuromuscular Junctions in a Dosage-Dependent Manner. Neuron 35, 291–306. 10.1016/s0896-6273(02)00769-9. [PubMed: 12160747]
74. Shen H, Zhu H, Panja D, Gu Q, and Li Z (2020). Autophagy controls the induction and developmental decline of NMDAR-LTD through endocytic recycling. Nat. Commun. 11, 2979. 10.1038/s41467-020-16794-5. [PubMed: 32532981]
75. Mao D, Lin G, Tepe B, Zuo Z, Tan KL, Senturk M, Zhang S, Arenkiel BR, Sardiello M, and Bellen HJ (2019). VAMP associated proteins are required for autophagic and lysosomal degradation by promoting a PtdIns4P-mediated endosomal pathway. Autophagy 15, 1214–1233. 10.1080/15548627.2019.1580103. [PubMed: 30741620]
76. Zhao YG, Liu N, Miao G, Chen Y, Zhao H, and Zhang H (2018). The ER Contact Proteins VAPA/B Interact with Multiple Autophagy Proteins to Modulate Autophagosome Biogenesis. Curr. Biol. 28, 1234–1245.e4. 10.1016/j.cub.2018.03.002. [PubMed: 29628370]
77. Fassio A, Falace A, Esposito A, Aprile D, Guerrini R, and Benfenati F (2020). Emerging Role of the Autophagy/Lysosomal Degradative Pathway in Neurodevelopmental Disorders With Epilepsy. Front. Cell. Neurosci. 14, 39. 10.3389/fncel.2020.00039. [PubMed: 32231521]
78. Ozturk-Colak A, Marygold SJ, Antonazzo G, Attrill H, Goutte-Gattat D, Jenkins VK, Matthews BB, Millburn G, Dos Santos G, Tabone CJ, and FlyBase C (2024). FlyBase: updates to the Drosophila genes and genomes database. Genetics 227, iyad211. 10.1093/genetics/iyad211. [PubMed: 38301657]
79. Shekhar S, Wert KJ, and Krämer H (2023). Visual Impairment Cell Non-autonomously Dysregulates Brain-wide Proteostasis (Cold Spring Harbor Laboratory).
80. Lee JJ, Sanchez-Martinez A, Zarate AM, Benincá C, Mayor U, Clague MJ, and Whitworth AJ (2018). Basal mitophagy is widespread in Drosophila but minimally affected by loss of Pink1 or parkin. JCB (J. Cell Biol.) 217, 1613–1622. 10.1083/jcb.201801044. [PubMed: 29500189]
81. Gratz SJ, Ukken FP, Rubinstein CD, Thiede G, Donohue LK, Cummings AM, and O'Connor-Giles KM (2014). Highly Specific and Efficient CRISPR/Cas9-Catalyzed Homology-Directed Repair in Drosophila. Genetics 196, 961–971. 10.1534/genetics.113.160713. [PubMed: 24478335]
82. Bruckner JJ, Zhan H, Gratz SJ, Rao M, Ukken F, Zilberg G, and O'Connor-Giles KM (2017). Fife organizes synaptic vesicles and calcium channels for high-probability neurotransmitter release. J. Cell Biol. 216, 231–246. 10.1083/jcb.201601098. [PubMed: 27998991]

83. Rueden CT, Schindelin J, Hiner MC, Dezonia BE, Walter AE, Arena ET, and Eliceiri KW. (2017). ImageJ2: ImageJ for the next generation of scientific image data. BMC Bioinf. 18, 529. 10.1186/s12859-017-1934-z.

84. Schindelin J, Arganda-Carreras I, Frise E, Kaynig V, Longair M, Pietzsch T, Preibisch S, Rueden C, Saalfeld S, Schmid B, et al. (2012). Fiji: an open-source platform for biological-image analysis. Nat. Methods 9, 676–682. 10.1038/nmeth.2019. [PubMed: 22743772]

85. Munnik T, and Wierzchowiecka M (2013). Lipid-binding analysis using a fat blot assay. Methods Mol. Biol. 1009, 253–259. 10.1007/978-1-62703-401-2_23.

86. Schneider CA, Rasband WS, and Eliceiri KW (2012). NIH Image to ImageJ: 25 years of image analysis. Nat. Methods 9, 671–675. 10.1038/nmeth.2089. [PubMed: 22930834]

Highlights

- In neurons, PDZD8 primarily localizes to ER-late endosome/lysosome membrane contact sites
- PDZD8 is required for activity-dependent synaptic growth
- PDZD8 promotes synaptic bouton formation through an autophagy-dependent mechanism
- PDZD8 promotes lysosome maturation and turnover to increase autophagic flux

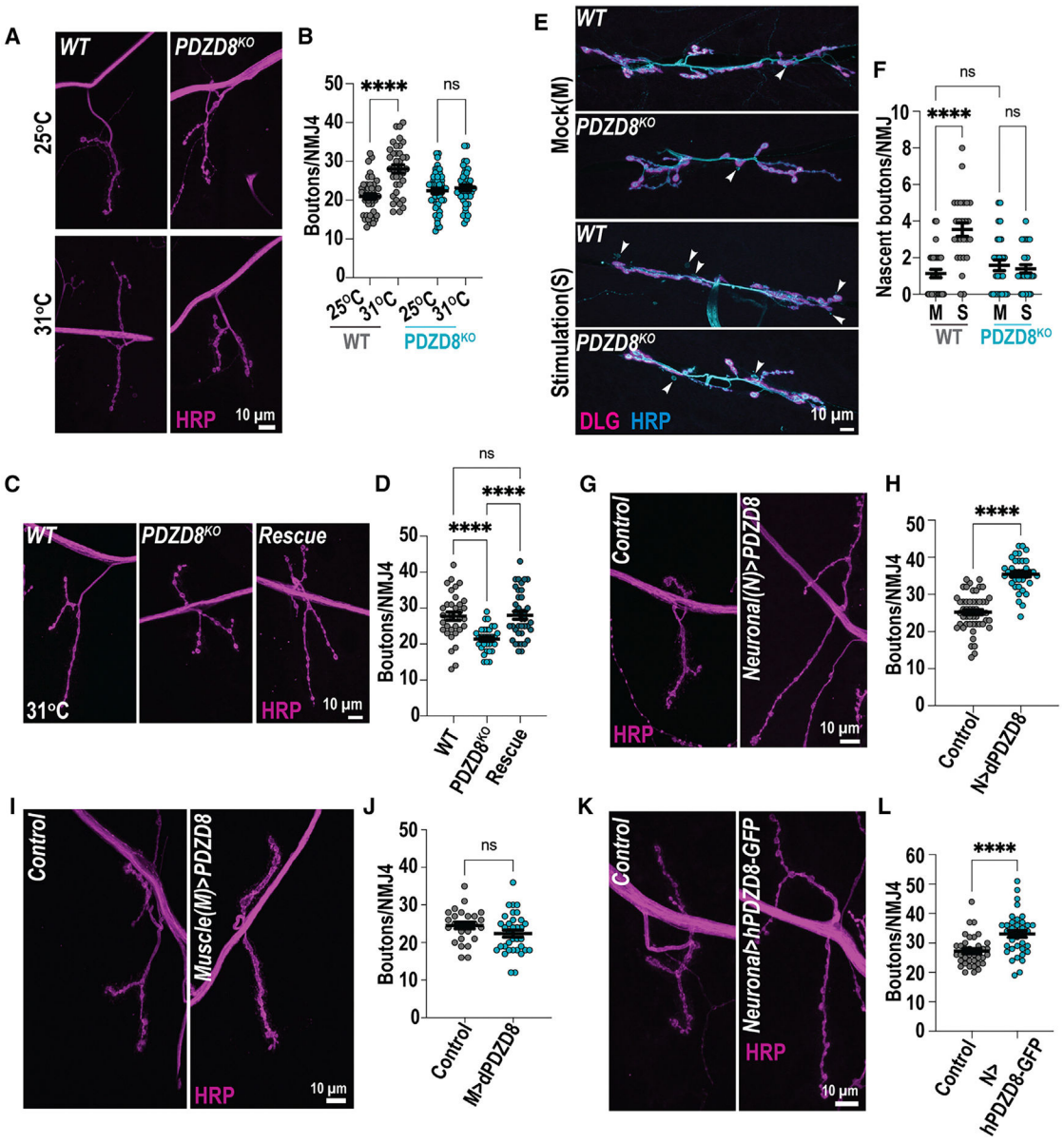

Figure 1. PDZD8 is required for activity-dependent synaptic bouton formation

(A–D) PDZD8 is dispensable for basal synapse formation (25°C), but required for activity-induced synaptic bouton formation (31°C). Representative confocal images of NMJs labeled with neuronal membrane marker FITC-conjugated anti-HRP (magenta) (A and C) and bouton quantification (B and D) in the indicated genotypes. Scale bar, 10 µm.

(E and F) PDZD8 is required for spaced high-K^+ stimulation-induced nascent bouton formation. Representative confocal images of NMJ 6/7 labeled with FITC-conjugated anti-HRP (cyan) and the postsynaptic density marker DLG (magenta) (E) and nascent bouton quantification (F) in the indicated genotypes. White arrows indicate DLG-negative nascent boutons. Scale bar, 10 µm.

(G–J) Neuronal overexpression of *Drosophila PDZD8* induces excess synaptic bouton formation, whereas muscle overexpression has no effect. Representative confocal images

of NMJs labeled with FITC-conjugated anti-HRP (magenta) (G and I) and bouton quantification (H and J) in the indicated genotypes. *elav-Gal4* was used to drive expression in neurons and *24B-Gal4* was used to drive expression in muscle. Scale bar, 10 μm.
(K and L) Human *PDZD8* (*hPDZD8*) misexpression in neurons leads to excess synaptic bouton formation. Representative confocal images of NMJs labeled with FITC-conjugated anti-HRP (magenta) (K) and bouton quantification (L) in the indicated genotypes. *elav-Gal4* was used to drive expression in neurons. Scale bar, 10 μm. Error bars represent mean ± SEM with significance calculated by two-way ANOVA followed by Tukey's multiple comparisons test (B, D, and F), unpaired t test (H and J), or Mann-Whitney U test (L). ****$p < 0.0001$; n.s., not significant.

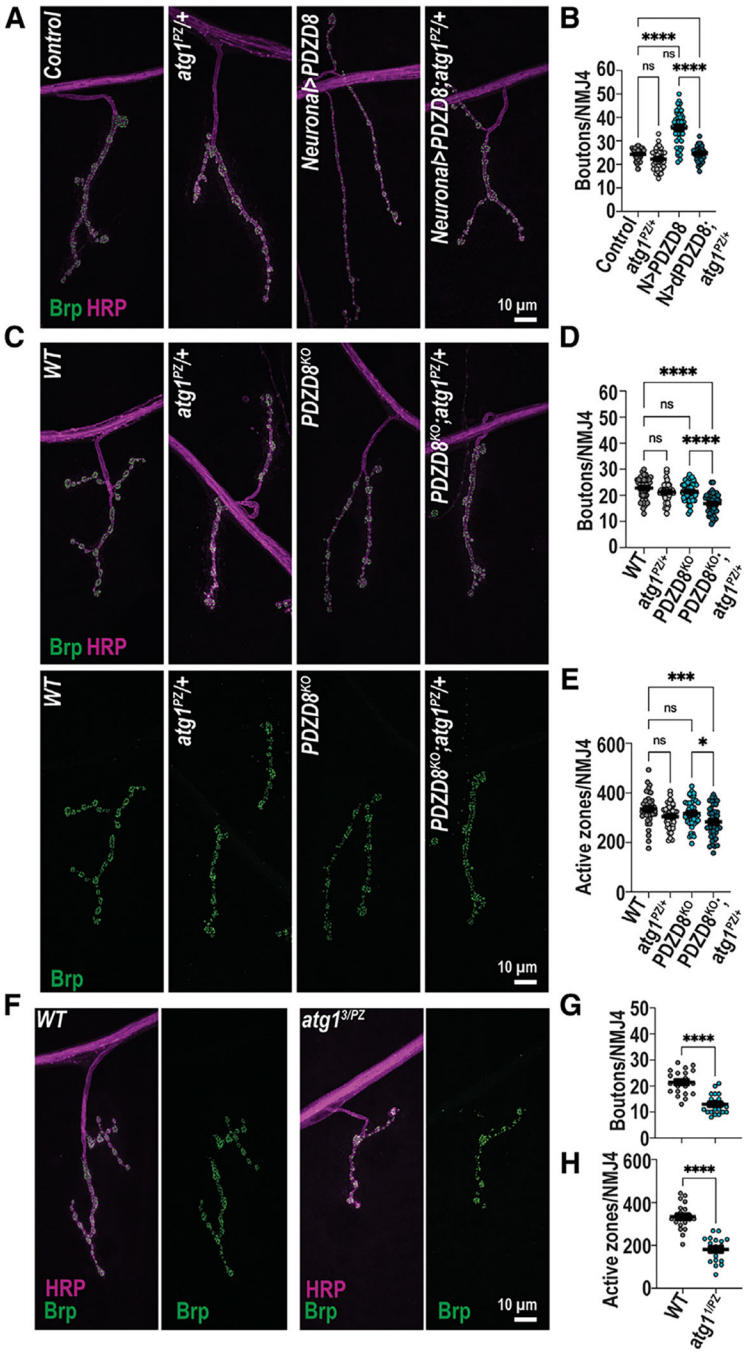

Figure 2. PDZD8 promotes synaptic growth via autophagy

(A–D) Downregulation of autophagy completely suppresses PDZD8-induced extra synaptic bouton formation and dominantly enhances the loss of *PDZD8,* leading to reduced synaptic bouton formation. Representative confocal images of NMJs co-labeled with antibodies against active zone marker Brp (green) and FITC-conjugated anti-HRP (magenta) (A and C) and bouton quantification (B and D) in the indicated genotypes. *elav-Gal4* was used to drive *PDZD8* expression in neurons.

(C and E) PDZD8-mediated autophagy regulates single synapse formation. The total number of active zones per NMJ 4 (E) in the indicated genotypes.

(F–H) Autophagy promotes bouton and synapse formation. Representative confocal images (F) co-labeled with antibodies against active zone marker Brp (green) and FITC-conjugated anti-HRP (magenta) and bouton (G) or active zone (H) number per NMJ 4 in the indicated genotypes. Scale bars, 10 μm. Error bars represent mean ± SEM with significance calculated by Kruskal-Wallis followed by Dunn's multiple comparisons test (B), ANOVA followed by Tukey's multiple comparisons test (D and E), or unpaired t test (G and H). $*p < 0.05$, $***p < 0.001$,$****p < 0.0001$; n.s., not significant.

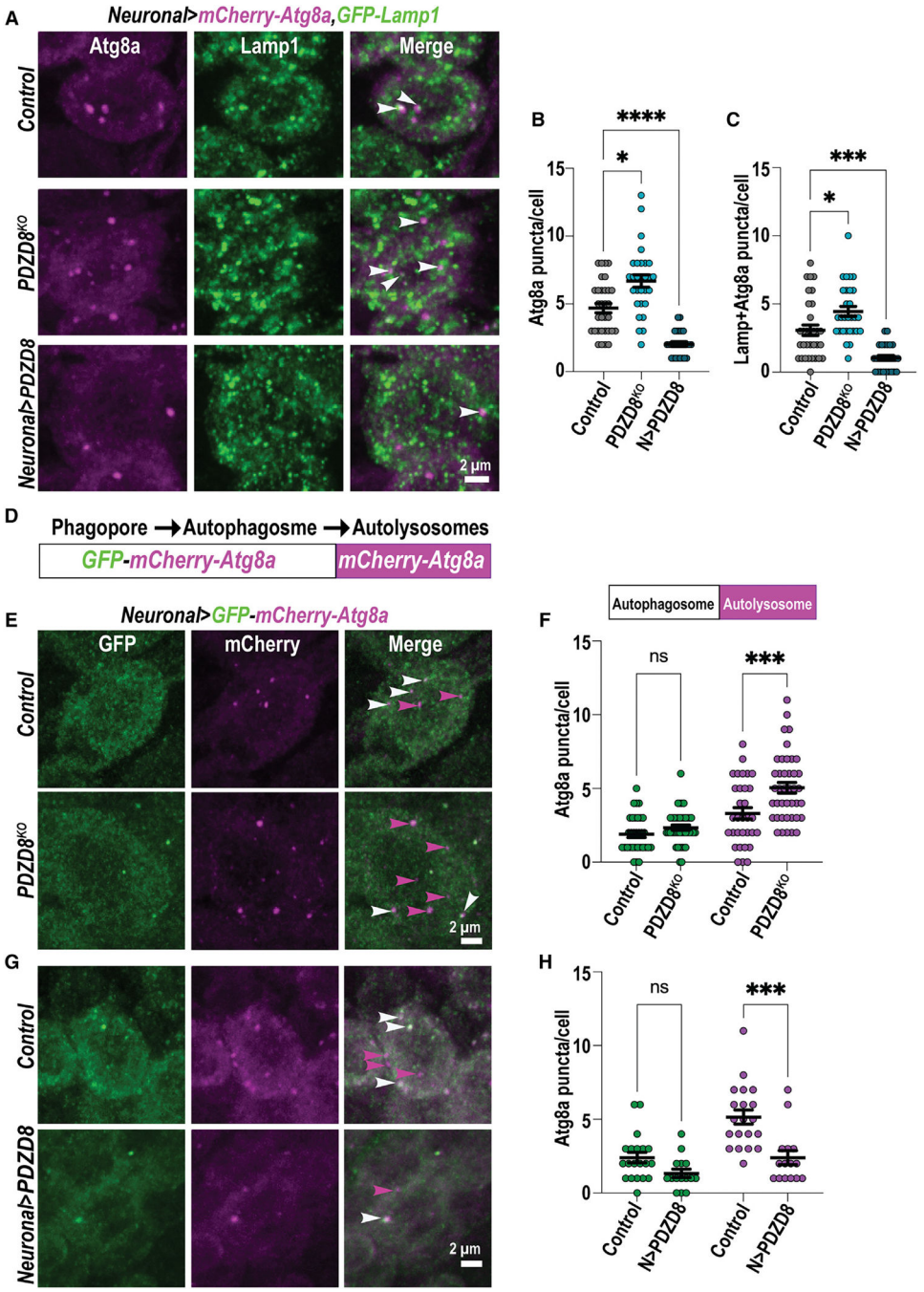

Figure 3. PDZD8 promotes autolysosomal turnover

(A–C) PDZD8 regulates autolysosome turnover. Confocal Z-projections of larval neuronal cell bodies co-labeled with antibodies against mCherry (magenta) and GFP (green) (A), quantification of Atg8a puncta (B), and quantification of Lamp1-positive Atg8a puncta (C) per cell in the indicated genotypes. White arrowheads indicate Lamp1-positive Atg8a structures. *elav-Gal4* was used to drive expression in neurons. Scale bar, 2 μm.

(D–H) The tandem-tagged Atg8a reporter (D) distinguishes autophagosomes from autolysosomes and can be used to assess autophagic flux. Confocal Z-projections of larval

neuronal cell bodies (E and F) co-labeled with antibodies against mCherry (magenta) and GFP (green) and quantification of Atg8a puncta (G and H) per cell in the indicated genotypes. White arrowheads point to Atg8a structures positive for both mCherry and GFP (autophagosomes) and magenta arrowheads point to Atg8a structures labeled by mCherry alone (autolysosomes). *elav-Gal4* was used to drive expression in neurons. Scale bars, 2 μm. Error bars represent mean ± SEM with significance calculated by ANOVA followed by Tukey's multiple comparisons test. *$p < 0.05$, ***$p < 0.001$, ****$p < 0.0001$; n.s., not significant.

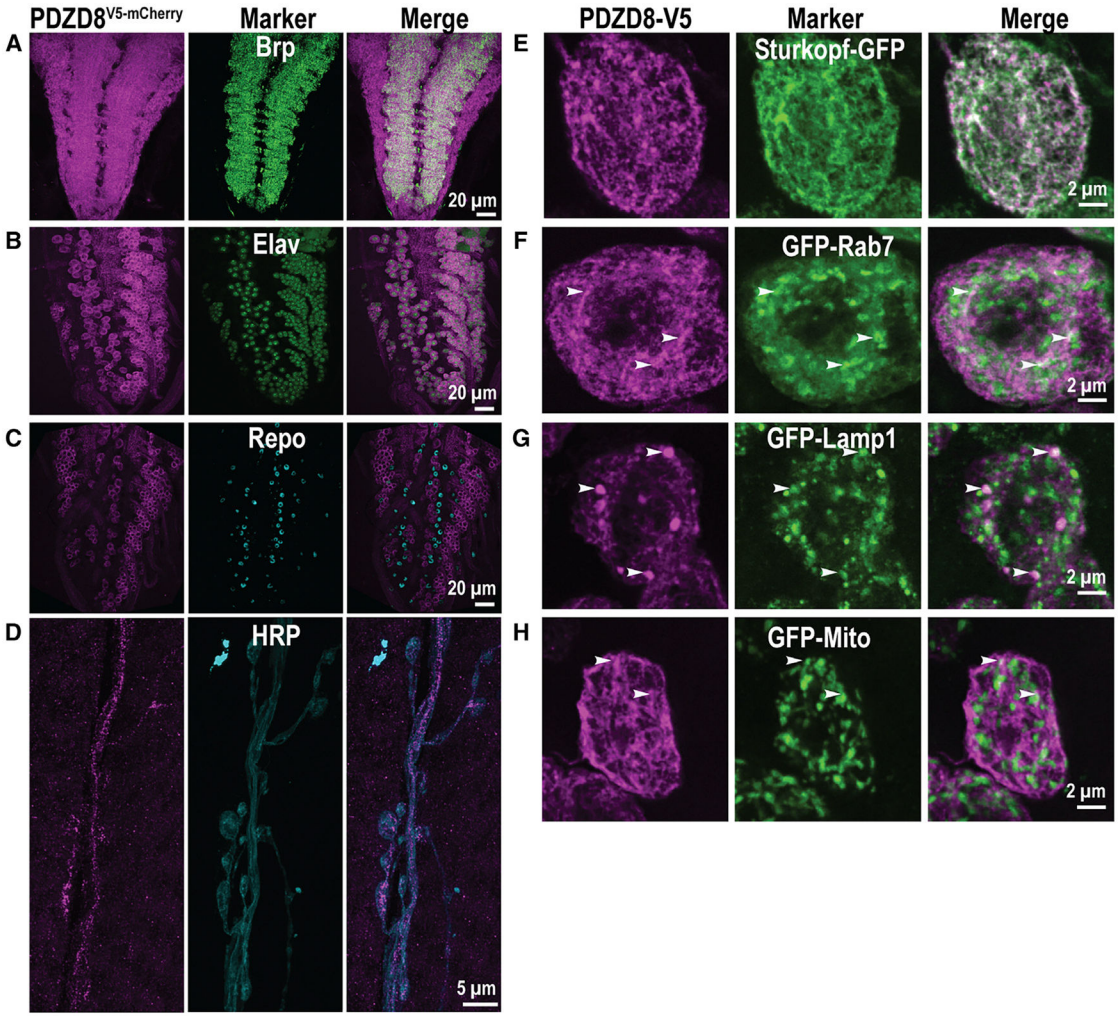

Figure 4. PDZD8 is enriched in neurons and localizes to ER-LEL MCSs

(A–C) PDZD8 is expressed in neurons and localized in cell bodies and at the synaptic neuropil. Confocal Z-projections of a *PDZD8*$^{V5\text{-}mCherry}$ larval ventral ganglia co-labeled with antibodies against mCherry (magenta) and the synaptic marker Brp (A) or neuronal cell marker Elav (B) in green, or the glial marker Repo in cyan (C). Scale bars, 20 μm.

(D) PDZD8 is expressed at the NMJ. Confocal Z-projections of a *PDZD8*$^{V5\text{-}mCherry}$ larval NMJ 6/7 co-labeled with antibodies against mCherry (magenta) and the neuronal membrane marker HRP (cyan). Scale bar, 5 μm.

(E–H) PDZD8 exhibits a reticular organization in neurons, co-localizing with ER and multiple MCSs. SoRa spinning disk deconvolved single plane of *elav-Gal4;PDZD8-V5* larval neuronal cell bodies co-labeled with antibodies against V5 (magenta) and in green neuronally expressed Sturkopf-GFP to label ER (E), GFP-Rab7 to label late endosomes (F), GFP-Lamp1 to label lysosomes (G), or GFP-Mito to label mitochondria (H). White arrowheads highlight sites of co-localization in (F–H). *elav-Gal4* was used to drive expression in neurons. Scale bars, 2 μm.

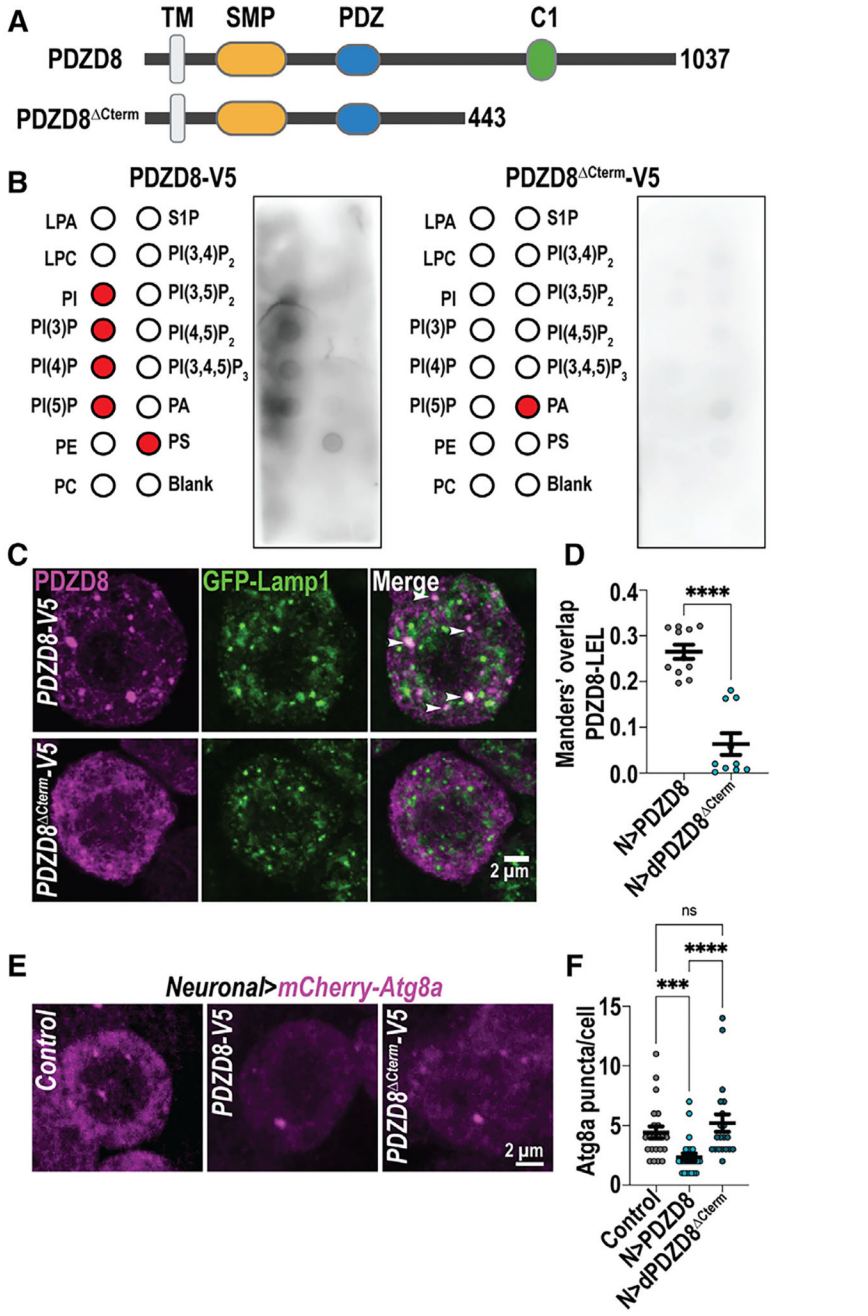

Figure 5. PDZD8 localization to ER-LEL MCSs is required to promote autophagy

(A) PDZD8 is a transmembrane (TM) protein with an SMP lipid-transfer domain at the N terminus followed by a PDZ protein-protein interaction domain and a C1 lipid-binding domain at the C terminus. Cartoon depicting the domain organization of full-length PDZD8 and the lipid-binding mutant with C terminus deleted (PDZD8$^{\Delta Cterm}$).

(B) PDZD8 interacts with lipids through the C terminus. Cartoon showing arrangement of lipids on the phosphatidylinositol phosphate (PIP) strip: lysophosphatidic acid (LPA), lysophosphocholine (LPC), phosphatidyinositol (PtdIns), phosphatidylinositol monophosphates PtdIns(3)P, s(4)P, PtdIns(5)P, phosphatidylethanolamine (PE),

phosphatidylcholine (PC), sphingosine-1-phosphate (S1P), phosphatidylinositol bisphosphate PtdIns(3,4)P_2, PtdIns(3,5) P_2, PtdIns(4,5)P_2, phosphatidylinositol bisphosphate PtdIns(3,4,5)P_3, phosphatidic acid (PA), and phosphatidylserine (PS). Red circles indicate lipid binding. PIP strips incubated with cellular extracts from *Drosophila* heads expressing full-length *PDZD8-V5* and *PDZD8$^{\Delta Cterm}$-V5*, respectively, and probed with antibodies against V5. Blots were developed together and imaged simultaneously. The immunoblot image presented for PDZD8$^{\Delta Cterm}$-V5 is taken at a higher exposure than PDZD8-V5 to reveal the background. Immunoblots at both exposures are included in STAR Methods, key resources table. *elav-Gal*4 was used to drive *PDZD8* transgene expression in neurons.
(C and D) PDZD8 is localized to ER-LELs MCSs through its C terminus. (C) SoRa spinning disk deconvolved single plane of neuronally expressed GFP-Lamp1 in *elav-Gal4; PDZD8-V5* and *elav-Gal4; PDZD8$^{\Delta Cterm}$-V5* larval neuronal cell bodies co-labeled with antibodies against GFP (green) and V5 (magenta). (D) Quantification of PDZD8 and PDZD8$^{\Delta Cterm}$ co-localization with lysosomes (LEL) using Mander's overlap coefficient.
(E and F) PDZD8 localization to ER-LEL MCSs is required to promote autophagy. Confocal Z-projections of larval neuronal cell bodies expressing *mCherry-Atg8* and labeled with antibodies against mCherry (magenta) (E) and Atg8a puncta quantification (F) in the indicated genotypes. *elav-Gal4* was used to drive expression in neurons. Scale bars, 2 μm. Error bars represent mean ± SEM with significance calculated by Mann-Whitney U test (D) or Kruskal-Wallis followed by Dunn's multiple comparisons test (F). ***$p < 0.001$, ****$p < 0.0001$; n.s., not significant.

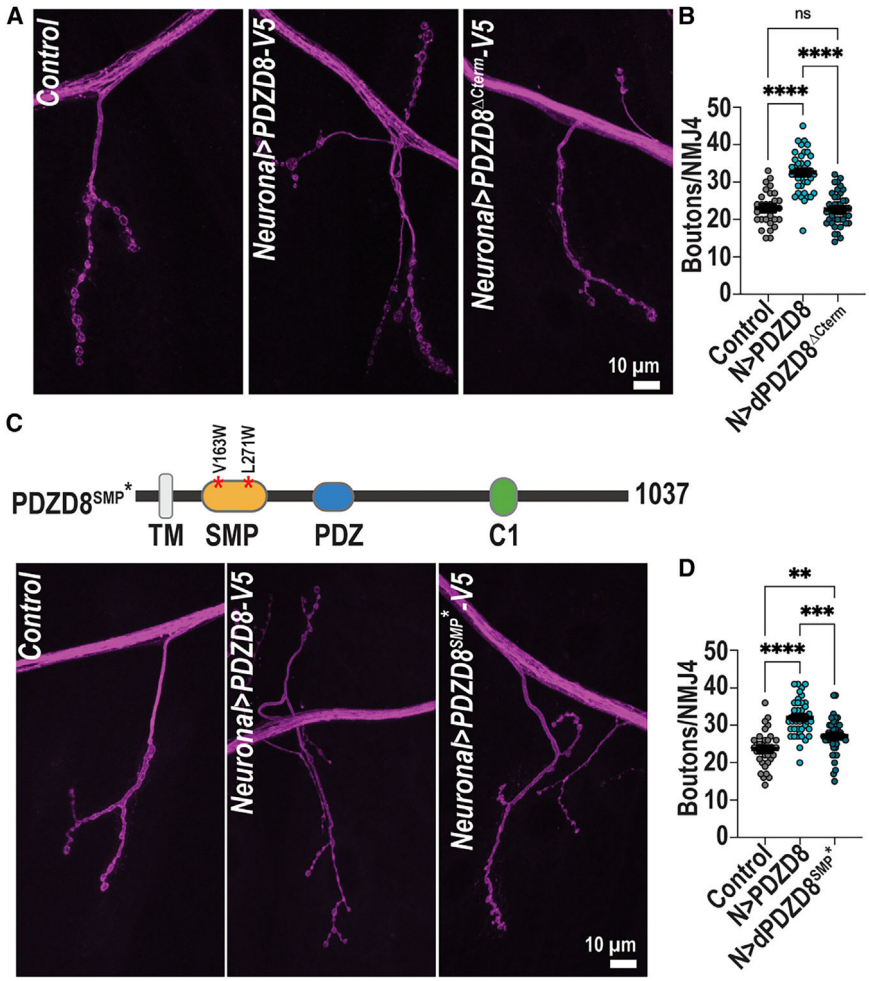

Figure 6. PDZD8 LEL localization and lipid transfer promote synaptic bouton formation

(A and B) ER-LEL MCS localization is critical for PDZD8-induced synaptic bouton formation. Representative confocal images of NMJs labeled with FITC-conjugated anti-HRP (magenta) (A) and bouton quantification (B) in the indicated genotypes. *elav-Gal4* was used to drive the *PDZD8* transgene expression in neurons.

(C and D) SMP domain mutations significantly impair PDZD8's ability to promote synaptic bouton formation. Representative confocal images of NMJs labeled with FITC-conjugated anti-HRP (magenta) (C) and bouton quantification (D) in the indicated genotypes. *elav-Gal4* was used to drive *PDZD8* transgene expression in neurons. Scale bars, 10 µm. Error bars represent mean ± SEM with significance calculated by ANOVA followed by Tukey's multiple comparisons test (B) or Kruskal-Wallis followed by Dunn's multiple comparisons test (D). $^{**}p < 0.01$, $^{***}p < 0.001$, $^{****}p < 0.0001$; n.s., not significant.

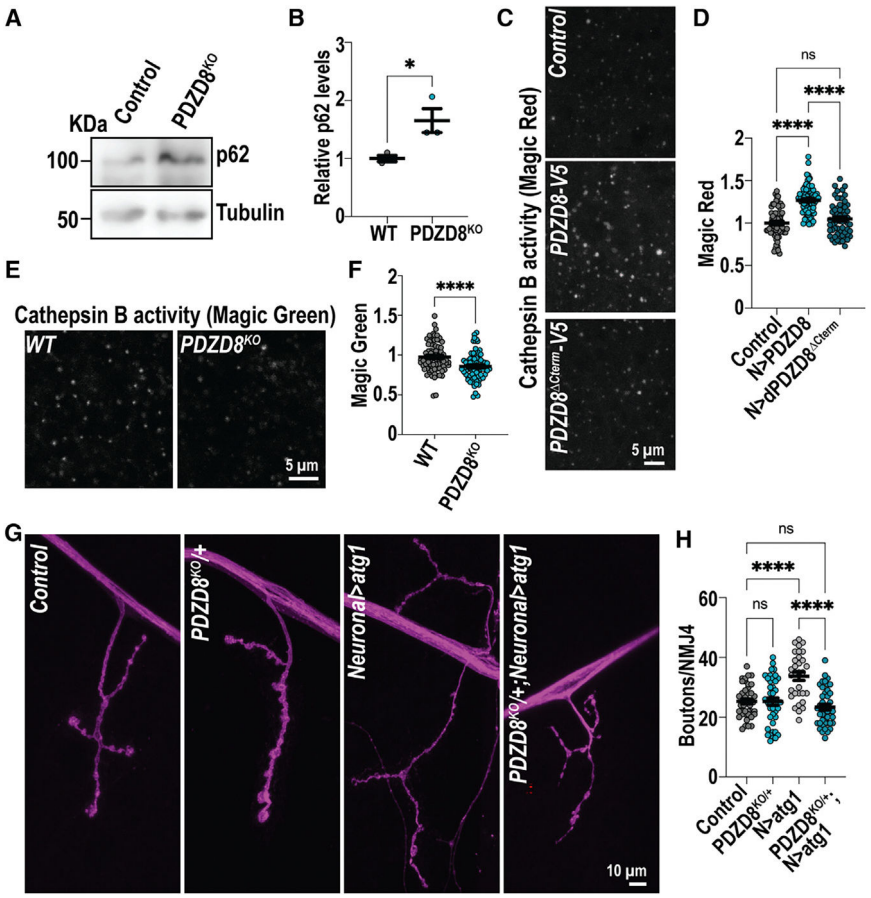

Figure 7. PDZD8 promotes LEL catalytic activity

(A and B) Immunoblot of *Drosophila* larval brain extracts labeled with an antibody against p62 (A). Tubulin is used for a loading control. Quantification of fold change in anti-p62 levels relative to WT control (B).

(C–F) PDZD8 promotes lysosome proteolytic activity. Representative confocal images of adult brains stained with Magic Green cresyl violet-(RR) 2 (C) and Magic Red cresyl violet-(RR)2 (E) to monitor lysosomal Cathepsin B enzymatic activity and quantification of normalized fluorescence intensity per neuron in the indicated genotypes. The same brain regions were used for quantification (D and F). *elav-Gal4* was used to drive expression in the neurons (E and F). Scale bars, 5 µm.

(G and H) PDZD8 is required for Atg1-induced excess bouton formation. Representative confocal images of NMJs labeled with FITC-conjugated anti-HRP (magenta) (G) and bouton quantification (H) in the indicated genotypes. *elav-Gal4* was used to drive *atg1* expression in neurons. Scale bar, 10 µm. Error bars represent mean ± SEM with significance calculated by Mann-Whitney test (B), ANOVA followed by Tukey's multiple comparisons test (D), or unpaired t test (F). *$p < 0.05$, ****$p < 0.0001$; n.s., not significant.

KEY RESOURCES TABLE

REAGENT or RESOURCE	SOURCE	IDENTIFIER
Experimental models: Organisms/strains		
w^{1118},$PDZD8^{V5\text{-}mCherry}$	This study	NA
w^{1118},*$PDZD8^{KO}$*	This study	NA
w^{1118};;UAS-PDZD8	This study	NA
w^{1118};;UAS-PDZD8-V5	This study	NA
w^{1118};;UAS-hPDZD8-GFP	This study	NA
w^{1118};;UAS-$PDZD8^{\Delta Cterm}$-V5	This study	NA
w^{1118};;UAS-$PDZD8^{SMP*}$ -V5	This study	NA
w^{1118}	O'Connor-Giles Lab outcrossed line	RRID:BDSC_3605
w; UAS-GFP-Mito	Bloomington Drosophila Stock Center	RRID: BDSC_25748
w; UAS-Sturkopf-GFP	Bloomington Drosophila Stock Center	RRID: BDSC_91394
w; UAS-GFP-Lamp1	Bloomington Drosophila Stock Center	RRID: BDSC_42714
w; UAS-GFP-Rab7	Bloomington Drosophila Stock Center	RRID: BDSC_42706
w; UAS-mCherry-Atg8a	Bloomington Drosophila Stock Center	RRID: BDSC_37750
w; UAS-GFP-mCherry-Atg8a	Bloomington Drosophila Stock Center	RRID: BDSC_37749
PDZD8 duplication ($w^{[1118]}$; Dp(1; 3)DC131, PBac(y[+mDint2] w[+mC] = DC131) VK00033)	Bloomington Drosophila Stock Center	RRID: BDSC_30272
w;P(PZ)$Atg1^{00305}$/TM6 (This stock has been rebalanced)	Bloomington Drosophila Stock Center	RRID: BDSC_11494
$Atg1^{3}$/TM6	Bloomington Drosophila Stock Center	RRID: BDSC_60732
$Syx17^{f03584}$/TM6	Bloomington Drosophila Stock Center	RRID: BDSC_85220
w; UAS-Atg1	Bloomington Drosophila Stock Center	RRID: BDSC_51655
w; OK6-Gal4	Bloomington Drosophila Stock Center	RRID: BDSC_64199
w, $elav^{C155}$-Gal4	Bloomington Drosophila Stock Center	RRID: BDSC_458
w; 24B-Gal4	Bloomington Drosophila Stock Center	RRID: BDSC_1767
w; UAS-mito-QC	Bloomington Drosophila Stock Center	RRID:BDSC_91641
Primers		
PDZD8KO-gRNA	CCAGCATGGAGATACCCATTTCAA	NA
PDZD8V5-mCherry gRNA	GATCATGGGCTACATGTCAATGGTT	NA
UAS-PDZD8-FP	GGAGAATTCATGGAGATACCCATTT CAAACATTCTG	NA

REAGENT or RESOURCE	SOURCE	IDENTIFIER
UAS-PDZD8-RP	GCAGGTACCCTACTGCAGCACCACA CCCTGGGC	NA
UAS-PDZD8-V5-FP	GGAGAATTCATGGAGATACCCATTTC AAACATTCTG	NA
UAS-PDZD8-V5-RP	CCTGAATTCATGGGTAAGCCTATCCCT AACCCTCTCCTCGGTCTCGATTCTACG GAGATACCCATTTCAAACATTCTG	NA
UAS-PDZD8DCterm-V5-FP	GGTAAGCCTATCCCTAACCCTC	NA
UAS-PDZD8DCterm-V5-RP	CTCGTACTTTTCGAAGTCCTCC	NA
UAS-PDZD8 V163W-V5-FP	GCACAACGTGTGGTTG GACAAGGATGAGC	NA
UAS-PDZD8 V163W-V5-RP	ACCGATAGCGACTTGACGTCC	NA
UAS-PDZD8 L271W-V5-FP	GAAACACACGTGGCCCAACTACAAGC	NA
UAS-PDZD8 L271W-V5-RP	CGGCGAACCGCCTTTCGGATC	NA
UAS-Cterm-FP	TGCGAATTCATGCACGACT TTGTGAGGACCCACT	NA
Antibodies		
Mouse anti-Bruchpilot	Developmental Studies Hybridoma Bank	Catalog # nc82; RRID: AB_2314866
RFP Antibody Pre-adsorbed (Rabbit Polyclonal)	Rockland	Catalog # 600–401-379; RRID: AB_2209751
Mouse anti-Discs Large	Developmental Studies Hybridoma Bank	Catalog # 4F3; RRID: AB_528203
Rat anti-Elav	Developmental Studies Hybridoma Bank	Catalog # Rat-Elav-7E8A10; RRID: AB_528218
Mouse anti-Repo	Developmental Studies Hybridoma Bank	Catalog # 8D12; RRID: AB_528448
Mouse anti-GFP	Developmental Studies Hybridoma Bank	Catalog # 12E6; RRID: AB_2617418
V5 Tag Monoclonal Antibody (Mouse)	Thermo Fisher Scientific	Catalog #R960–25; RRID:AB_2556564
ChromoTek RFP Monoclonal antibody (5F8) (Rat)	ChromoTek	Catalog # 5f8; RRID: AB_2336064
Mouse anti-tubulin	Developmental Studies Hybridoma Bank	Catalog #E7; RRID: AB_2315513
Rabbit anti-p62	Helmut Kramer[79]	NA
GFP Polyclonal Antibody, Alexa Fluor™ 488	Thermo Fisher Scientific	Catalog #A-21311; RRID: AB_221477

REAGENT or RESOURCE	SOURCE	IDENTIFIER
Goat anti-Mouse IgG (H + L) Highly Cross-Adsorbed Secondary Antibody, Alexa Fluor™ 488	Thermo Fisher Scientific	Catalog #A-11029; RRID: AB_2534088
Goat anti-Rabbit IgG (H + L) Highly Cross-Adsorbed Secondary Antibody, Alexa Fluor™ 488	Thermo Fisher Scientific	Catalog #A-11034; RRID: AB_2576217
Goat anti-Mouse IgG (H + L) Highly Cross-Adsorbed Secondary Antibody, Alexa Fluor™ 568	Thermo Fisher Scientific	Catalog #A-11031; RRID: AB_144696
Goat anti-Rabbit IgG (H + L) Highly Cross-Adsorbed Secondary Antibody, Alexa Fluor™ 568	Thermo Fisher Scientific	Catalog #A-11036; RRID: AB_10563566
Goat anti-Rat IgG (H + L) Cross-Adsorbed Secondary Antibody, Alexa Fluor™ 568	Thermo Fisher Scientific	Catalog #A-11077; RRID: AB_2534121
Goat anti-Mouse IgG (H + L) Highly Cross-Adsorbed Secondary Antibody, Alexa Fluor™ 647	Thermo Fisher Scientific	Catalog #A-21236; RRID: AB_2535805
Goat anti-Rabbit IgG (H + L) Highly Cross-Adsorbed Secondary Antibody, Alexa Fluor™ 647	Thermo Fisher Scientific	Catalog # A-21245; RRID: AB_2535813
Goat anti-Rat IgG (H + L) Cross-Adsorbed Secondary Antibody, Alexa Fluor™ 647	Thermo Fisher Scientific	Catalog #A-21247; RRID: AB_141778
Alexa Fluor® 647 AffiniPure Goat AntiHorseradish Peroxidase	Jackson ImmunoResearch Labs	Catalog# 123–605-021; RRID: AB_2338967
Peroxidase AffiniPure Goat Anti-Mouse IgG (H + L)	Jackson ImmunoResearch Labs	Catalog# 115–035-003; RRID: AB_10015289
Peroxidase AffiniPure Donkey Anti-Rabbit IgG (H + L) (min X Bov, Ck, Gt, GP, Sy Hms, Hrs, Hu, Ms, Rat, Shp Sr Prot)	Jackson ImmunoResearch Labs	Catalog # 711–035-152; RRID: AB_10015282
Peroxidase AffiniPure Goat Anti-Rat IgG (H + L) (min X Hu, Bov, Hrs, Rb Sr Prot)	Jackson ImmunoResearch Labs	Catalog# 112–035-143; RRID: AB_2338138
Chemicals		
Bouin's fixative	Sigma Aldrich	Catalog #HT10132
Vectashield	Vector Laboratories	Catalog # H-1000–10
ProLong™ Glass Antifade Mountant	ThermoFisher Scientific	Catalog #P36980
Antibiotic-Antimycotic (100X)	ThermoFisher Scientific	Catalog # 15240062
Schneider's Drosophila Medium	ThermoFisher Scientific	Catalog #21720024
Recombinant DNA/Plasmids/Cell lines		
LD34222 (PDZD8 cDNA Gold clone)	Drosophila Genomic Resource Center	Catalog# 12606; RRID: DGRC_12606
hPDZD8-GFP	Pietro De Camilli Lab[11]	NA
UAS-PDZD8-V5	This study	NA

REAGENT or RESOURCE	SOURCE	IDENTIFIER
UAS-hPDZD8-GFP	This study	NA
UAS-PDZD8$^{\Delta Cterm}$-V5	This study	NA
UAS-PDZD8^{smp*} -V5	This study	NA
UAS-Cterm-V5	This study	
LAMP1-GFP	Addgene	Catalog# 16290
pAC-GAL4 (Actin-Gal4)	Addgene	Catalog # 24344
Schneider's Line S2 FBtc0000181 (S2-DRSC)	Drosophila Genomic Resource Center	Catalog # 181; RRID:CVCL_Z992
Commercial assays/kits		
Magic Red® Cathepsin-B Assay Kit	ImmunoChemistry Technologies	Catalog # SKU: 937
Magic Green® Cathepsin-B Assay Kit	ImmunoChemistry Technologies	Catalog #SKU: 9151
SuperSignal™ West Femto Maximum Sensitivity Substrate	Thermo Fisher Scientific	Catalog # 34095
Effectene Transfection Reagent	Qiagen	Catalog # 301425
Software		
Adobe Photoshop	Adobe Systems	RRID:SCR_014199
Adobe Illustrator	Adobe Systems	RRID:SCR_010279
ImageJ	NIH	RRID: SCR_003070
Prism	GraphPad Software, Inc	RRID: SCR_002798
NIS-Elements	Nikon	RRID: SCR_002776
ApE Plasmid Editor	https://jorgensen.biology.utah.edu/wayned/ape/	RRID:SCR_014266
BioRender	http://biorender.com	RRID:SCR_018361